iScience

CellPress
OPEN ACCESS

Article

Efficient proximal tubule-on-chip model from hiPSC-derived kidney organoids for functional analysis of renal transporters

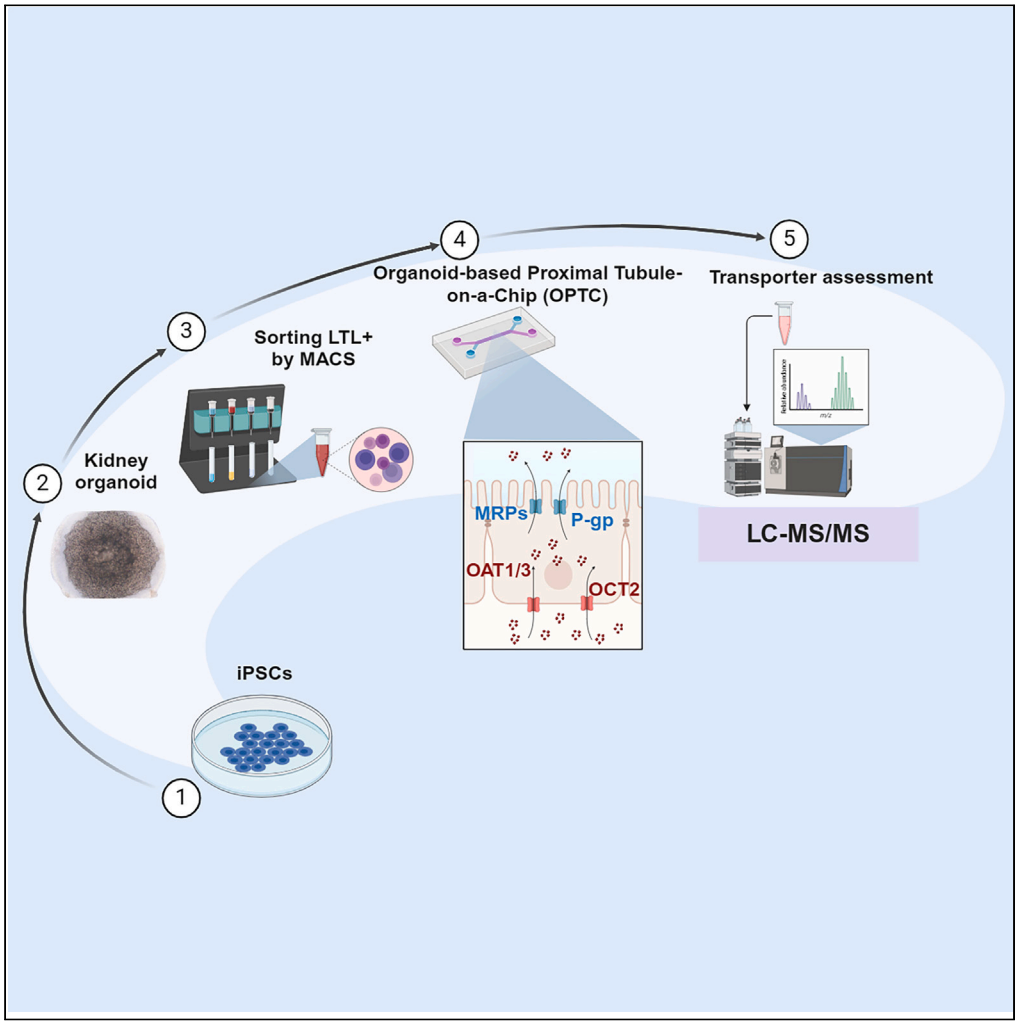

Cheng Ma (马成), Ramin Banan Sadeghian, Ryosuke Negoro (根来亮介), ..., Naoki Ishiguro (石黒直樹), Minoru Takasato (髙里実), Ryuji Yokokawa (横川隆司)

yokokawa.ryuji.8c@kyoto-u.ac.jp

Highlights

Developed a hiPSC-derived kidney organoid-based proximal tubule-on-chip model

Enhanced expression and polarity of OAT1/3 compared to immortalized cells

Demonstrated improved efflux and uptake transport functionality

Provides a reliable platform for assessing human renal transporters

Ma et al., iScience 27, 110760
September 20, 2024
https://doi.org/10.1016/j.isci.2024.110760

iScience

CellPress
OPEN ACCESS

Article

Efficient proximal tubule-on-chip model from hiPSC-derived kidney organoids for functional analysis of renal transporters

Cheng Ma (马成),[1] Ramin Banan Sadeghian,[1] Ryosuke Negoro (根来亮介),[2] Kazuya Fujimoto (藤本和也),[1] Toshikazu Araoka (荒岡利和),[3] Naoki Ishiguro (石黒直樹),[4] Minoru Takasato (髙里実),[5,6,7] and Ryuji Yokokawa (横川隆司)[1,8,*]

SUMMARY

Renal transporters play critical roles in predicting potential drug-drug interactions. However, current *in vitro* models often fail to adequately express these transporters, particularly solute carrier proteins, including organic anion transporters (OAT1/3), and organic cation transporter 2 (OCT2). Here, we developed a hiPSC-derived kidney organoids-based proximal tubule-on-chip (OPTC) model that emulates *in vivo* renal physiology to assess transporter function. Compared to chips based on immortalized cells, OPTC derived from the two most commonly used differentiation protocols exhibited significant improvement in expression level and polarity of OAT1/3 and OCT2. Hence, the OPTC demonstrates enhanced functionality in efflux and uptake assessments, and nephrotoxicity. Furthermore, these functionalities are diminished upon adding inhibitors during substrate-inhibitor interactions, which were closer to *in vivo* observations. Overall, these results support that OPTC can reliably assess the role of renal transporters in drug transport and nephrotoxicity, paving the way for personalized models to assess renal transport and disease modeling.

INTRODUCTION

It is well established that solute carrier proteins (SLCs) expressed in the membrane of renal tubule cells play a major role in the disposition and elimination of xenobiotics. They also facilitate the transport of solutes containing ions and metabolites peptides, across renal epithelial barriers.[1,2] Among these proteins, OAT1 and OAT3 take the king's share of organic transporters managing the transport of endogenous and exogenous anions, thus improving renal clearance of drugs such as adefovir, PAH, and rosuvastatin Ca. OCT2 on the other hand, is responsible for the elimination of cation-coupled drugs including but not limited to Cisplatin and Metformin. Abnormalities in these transporters are linked to significant renal disorders and altered drug dynamics. Regulatory bodies, including the US Food and Drug Administration (FDA),[2] the European Medicines Agency (EMA),[3] and the Pharmaceuticals and Medical Devices Agency (PMDA)[4] have thus highlighted these transporters as focal points in drug interaction research.

The proximal tubule (PT),[5] a segment of the nephron's tubular network beginning from the pole of the renal corpuscle, plays a crucial role in renal physiology. It is mainly responsible for the reabsorption of a substantial proportion of nutrients into the adjacent peritubular capillary network. Being equipped with a plethora of uptake and efflux transporters, it is central to the management of xenobiotics, marking it a primary site for both substance processing and potential toxicity. The SLC transporters play a crucial role in the renal handling of drugs by facilitating their uptake and secretion. These transporters are crucial for drug absorption from the blood into renal tubule cells and subsequent excretion into the urine. Their precise functioning is essential for maintaining drug homeostasis in the body and avoiding potential adverse effects. As a result, designing *in vitro* models for the organ that features these transporters and could provide clinically relevant data becomes crucially important.

It so happens that previous *in vitro* models have not succeeded in faithfully incorporating and studying these transporters.[6–10] It is mainly because primary cells rapidly lose expression of these vital transporters post-cultivation, and most immortalized cells do not efficiently express them. In cases where OATs[11,12] and OCT2[13] were expressed, genetically modified immortalized cells were typically utilized, starkly

[1]Department of Micro Engineering, Kyoto University, Kyoto 615-8540, Japan
[2]Laboratory of Molecular Pharmacokinetics, College of Pharmaceutical Sciences, Ritsumeikan University, Kusatsu 525-8577, Japan
[3]Center for iPS Cell Research and Application (CiRA), Kyoto University, Kyoto 606-8507, Japan
[4]Pharmacokinetics and Non-Clinical Safety Department, Nippon Boehringer Ingelheim Co. Ltd, Kobe, Japan
[5]RIKEN Center for Biosystems Dynamics Research (BDR), Kobe 650-0047, Japan
[6]Graduate School of Medicine, Osaka University, Suita 565-0871, Japan
[7]Graduate School of Biostudies, Kyoto University, Kyoto 606-8501, Japan
[8]Lead contact
*Correspondence: yokokawa.ryuji.8c@kyoto-u.ac.jp
https://doi.org/10.1016/j.isci.2024.110760

contrasting with authentic *in vivo* cells. Stem cells, notably those derived from human induced pluripotent stem cells (hiPSCs), offer competent replication and superior in vivo-like properties. These cells are differentiated into a spectrum of kidney cell types through a variety of protocols, thus circumventing ethical dilemmas tied to embryonic renal progenitor cells and surpassing the limitations inherent in traditional models.

For example, Takasato et al.'s approach,[14] inducing multiple progenitors simultaneously, results in organoids featuring nephron segments linked to collecting ducts, encapsulated within an interstitial matrix and vasculature. Tsujimoto et al.,[15] on the other hand, have refined this process by separately cultivating mesoderm lineages, yielding organoids that more accurately represent embryonic kidney development, including nephrogenic niches and vascularized, interconnected renal structures.

The assessment of physiological function of kidney organoids is challenging due to their structure, thickness, and tissue complexity.[16] The incomplete polarization[17,18] also limited the kidney function assessment in such 3D complex structures. Although transporter functional assays are reported using kidney organoids,[16] the substrate of Rhodamine 123 is not exclusively transported by P-gp but also BCRP[19] and MRPs.[20] Additionally, it was challenging to confirm tight junction integrity nor differentiate between active transport and passive diffusion in organoids. Moreover, even with the use of organoid-derived PT cells, the 3D bioprinted proximal tubule model[21] only assessed nephrotoxicity using aristolochic acid, a non-specific substrate taken up by both OAT1 and OAT3. This model did not include a quantitative analysis of vectorial transport across the proximal tubule layer or the efflux transport process, which are crucial for a preclinical tool used in drug development.

To address these challenges, we report a micro-physiological system (MPS), the "Proximal Tubule-on-Chip" (PToC), which provides fit-for-purpose platforms integrating with proximal tubule epithelial cells sorting from hiPSC-derived kidney organoids (LTL+ cells). This system aims to model renal physiology more accurately and predict transporter-mediated drug interactions in a setting that closely mimics *in vivo* conditions. The confluent, tightly packed monolayer in our system demonstrates correct apical and basal polarization, enabling personalized assessment of drug transcellular function and toxicity. The selection of an appropriate organoid source is crucial for establishing a high-functioning PToC model. Therefore, we utilized two widely used kidney organoid protocols developed by Takasato et al.[14] and Tsujimoto et al.[15] The LTL+ cells derived from these protocols, when seeded into the PToC exhibited significant improvement in the expression level of OAT1/3 and OCT2, enhancing drug transport in comparison to control chips with immortalized proximal tubule epithelial cells (RPTEC PToC). Ultimately, we assess the uptake and transcellular transport of substrates mediated by OAT1/3 in the presence or absence of inhibitors, along with the functionality of the OCT2 and efflux transporter multidrug toxin extrusion (MATE1) and P-glycoprotein (P-gp). In the present study, an OPTC was established using LTL+ cells from hiPSC-derived kidney organoids to assess the human renal transporters, paving the way for the application of hiPSC and the personalized models.

RESULTS

Characterization of organoid-derived proximal tubule epithelial cells cultivated in the PToC

The development of the MPS incorporating proximal tubule cells, hereafter referred to as the PToC entails a series of intricate steps: (1) Differentiation of iPSCs into nephron progenitor cells; (2) Harvesting and pelleting these cells onto transwell filters for maturation into organoids[14,15]; (3) Dissociation of these organoids into cell suspensions, exposure to Lotus Tetragonolobus Lectin (LTL), a brush border maker, and subjection to Magnetic-Activated Cell Sorting (MACS)[10]; (4) Expansion of LTL+ cells in dish culture; and (5) Seeding of the LTL+ cells onto porous polyester membranes, pre-coated with laminin-511 as an extracellular matrix (ECM), in the top channel of our PToC device (Figure 1A).

Proximal tubule epithelial cells were identified within the organoids by their expression of EpCAM (an epithelial cell marker), LTL, and more specifically, the albumin transporter megalin (Figure 1C). Each protocol exhibited robust expression of SLC protein family transporters, particularly those related to OATs, OCT2, and their associated efflux pumps, which are of primary interest in our study. Re-analysis of bulk RNA-seq dataset obtained from previous studies[22] revealed that the organoid developed by Tsujimoto et al.,[15] demonstrated enhanced expression of OAT1, OAT3, and related transporters BCRP, and MRP2, in comparison to the organoid that developed by Takasato et al.[14,23] Similarly, Takasato et al. showed superior expression of MRP4, MATE2, and other related transporters (Figure 1B) compared to Tsujimoto et al. As those gene expression data were generated using whole organoids rather than purified PT cells, we performed immunofluorescent imaging analysis in both organoids and confirmed the expression of OAT1, OAT3, OCT2, and MATE1 in PT cells through confocal fluorescent imaging of tissue-cleared samples (Figure S1), and more detailed analysis in cryo-sectioned specimens (Figure 1D).

Based on our previous research,[10] LTL emerged as the most effective marker for isolating proximal tubule epithelial cells from organoids, with MACS being a more benign method compared to fluorescence-activated cell sorting (FACS) via flow cytometry.

After MACS isolation, LTL+ cells (#1-LTL+, dissociated from organoids developed by Takasato et al.; #2-LTL+, dissociated from organoids developed by Tsujimoto et al.) were expanded through a single passage in Petri dish culture before seeding onto the device (Figure 2A). Exploring optimal growth conditions, the LTL+ cells were cultured on uncoated Petri dishes, FNC Coating Mix (FNC)-coated, and iMatrix-511 coated substrate. Our findings indicated that the commonly used FNC coating in proximal tubule (PT) cell culture did not provide an ideal environment, often leading to LTL+ cells adopting a fibroblast-like morphology instead of the desired proximal tubule phenotype. Contrastingly, iMatrix-511, a substrate traditionally used in iPSC culture, facilitated rapid growth rates, resulting in LTL+ cells that more accurately resembled the cuboidal phenotype of cultured immortalized proximal tubule cells (Figure 2B).

When LTL+ cells were cultured on porous polyester membranes within the device, we observed that cells on FNC-coated surfaces tended to detach, whereas iMatrix-511 coated surfaces supported the formation of a confluent and tight cellular layer (Figure S4B). Therefore, LTL+ cells were cultured on iMatrix-511 coated substrates for one-time passage, where passage 1 denotes LTL+ cells freshly isolated from kidney organoids, to increase their stability and proliferative capacity after MACS. Subsequent to this one-time passage, the cells displayed good

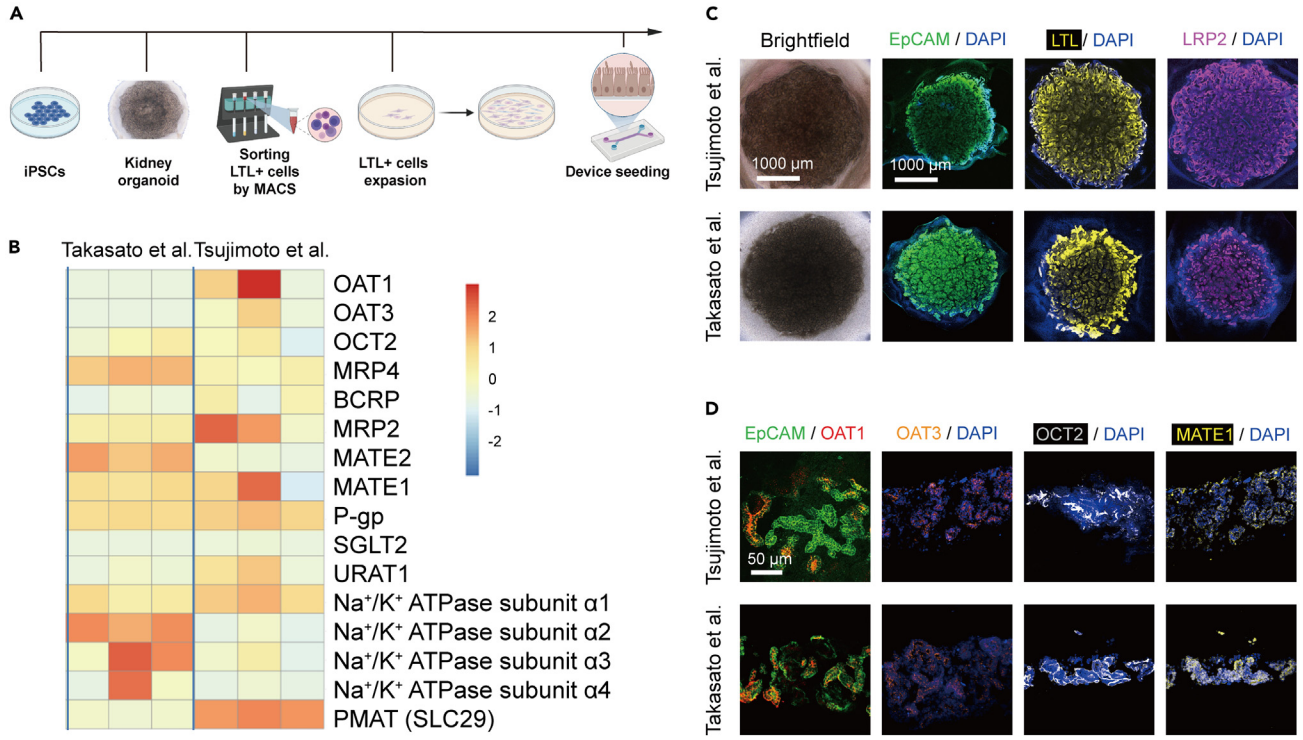

Figure 1. Appearance of proximal tubule cells in hiPSC-derived kidney organoids

(A) Schematic overview of establishing hiPSC-derived kidney organoids sourcing proximal tubule epithelial cell-on-chip models.

(B) Heatmap comparing transporter expression of two types of hiPSC-derived kidney organoids. Three boxes in line per protocol represent replicates from different experiments.

(C) Select brightfield and confocal fluorescent images (z-intensity projected) of 4A6 kidney organoids (tissue-cleared) on day 27 and CRL 1502.3 kidney organoids (tissue-cleared) on day 22. Immunochemistry is for EpCAM and proximal tubule markers, LTL, and LRP2 (megalin), scale bars represent 1000 μm.

(D) Confocal images of 4A6 kidney organoid (cryo-sectioned) on day 27 and CRL 1502.3 kidney organoid (cryo-sectioned) on day 22 stained for OAT1, EpCAM, OAT3, OCT2, and MATE1 in nephron segments, scale bars represent 50 μm.

expression of PT markers and tight junction (Figure S2). And a detailed gene expression analysis revealed nuanced changes. Specifically, certain transporter genes exhibited a marginal decrease in expression levels, albeit within permissible limits. Conversely, other genes showed no significant alteration, or in some cases, an enhanced expression profile (Figure S3). Concurrently, a comparative analysis at the gene level between two distinct organoid types was performed, focusing on transporter gene expression post-dish culture. This comparison demonstrated a correlation with the organoid-level observations, as depicted in Figure 1B.

After the initial culturing phase, LTL+ cells were seeded onto iMatrix-511 pre-coated membranes within the upper channel of our PToC (Figure S4A). The seeding density was maintained at a minimum of 1.5×10^7 cells/mL. Remarkably, within a span of just 5 days, these OPTCs (#1-LTL+ PToC and #2-LTL+ PToC) developed into confluent and tightly packed layers. They strongly expressed epithelial markers such as EpCAM, LTL, and megalin, surpassing even the RPTEC PToC (control) in the expression of LTL and megalin (Figure 2C). In stark contrast, LTL– cells, while forming confluent layers, lacked any expression of these key epithelial markers (Figure S4C).

Further examination involved assessing the expression of ZO-1, a tight junction protein, and conducting FITC-inulin perfusion to evaluate barrier function. The LTL+ cells demonstrated ZO-1 expression levels comparable to those in the RPTEC PToC (Figure 2C). Additionally, we observed that their diffusional permeability closely matched that of the RPTECs in the PToC (Figures 2D and S4D). These findings indicate that our OPTCs are not only structurally robust but also functionally competent, showcasing the potential for detailed studies on polarized drug intracellular uptake, transcellular transport, and related toxicity. Through this comprehensive approach, we established a robust PToC model using LTL+ cells extracted from hiPSC-derived kidney organoids, demonstrating its potential for advanced studies in renal physiology and drug transport dynamics.

Enhanced expression and polarization of functional OAT1/3 in OPTCs

Our study delved into OPTC, with a focus on evaluating the expression of crucial drug transporters, OAT1 and OAT3. After a five-day culture, immunostaining experiments indicated a more pronounced expression of both OAT1 and OAT3 in OPTCs in comparison with RPTEC PToC, as illustrated in Figures 3A and S5A. Crucially, cell polarity plays a pivotal role in MPS, especially in assessing vectorial transport and toxicity. Effective transporter function depends on the polarity of the transporter expression.

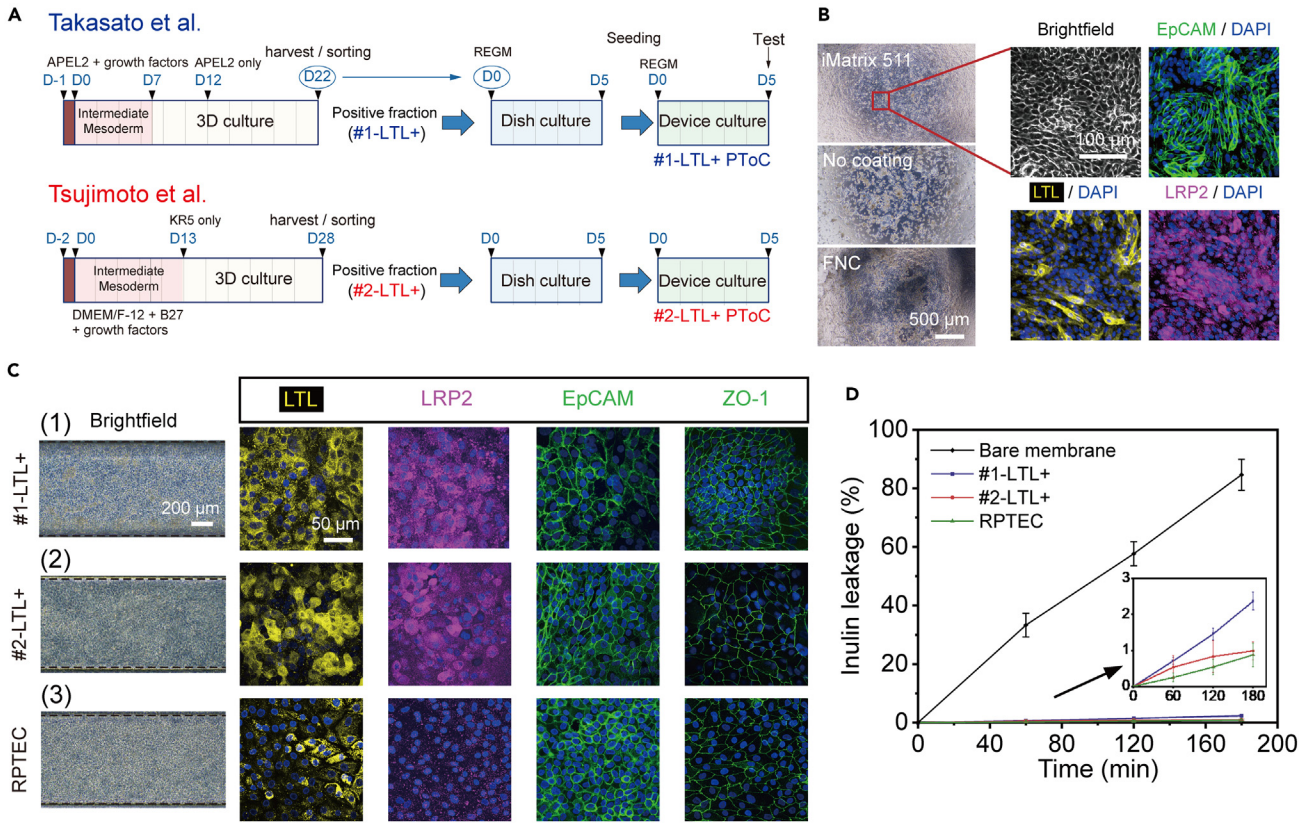

Figure 2. Application of hiPSC-derived kidney organoids in on-chip modeling of PToC

(A) The simplified protocol of hiPSC differentiation into intermediate mesoderm and formation of 3D kidney organoids, followed by dissociation, sorting, expansion, and seeding of the LTL+ cells (refer to dissociated organoid cells, positive fraction of MACS) on the device.

(B) Brightfield images showing #1-LTL+ cells grown without coating, with FNC coating and iMatrix 511 coating on the dish, respectively. Higher magnification, the confocal image of #1-LTL+ cells cultured on iMatrix 511 coating which stained for EpCAM, LTL+, and LRP2 (megalin), scale bars represent 500 μm and 200 μm, respectively.

(C) Brightfield images showing the evolution of #1-LTL+, #2-LTL+, and RPTEC cells on devices, scale bars represent 200 μm. The confocal image of three types of cells cultured on devices that stained for LTL+, LRP2 (megalin), EpCAM, and ZO-1, scale bars represent 50 μm.

(D) FITC-labeled inulin (3000 Da < MW < 6000 Da), applied at 100 g mL^{-1} to the top channel (apical side) and measured at the bottom on day 5 for three types of devices and controlled by the bare membrane. The impermeability of the tissue layers to inulin confirms the epithelial barrier function. Data are represented as mean ± SD ($n \geq 3$).

In kidney organoids, we observed a lack of proper polarization in both organic cation and anion transporters (Figures S1 and 1D). Given that our LTL+ cells originated from these organoids, we investigated whether culturing on a 2D membrane could enhance the polarization of OAT1 and OAT3. Through comprehensive immunofluorescence studies, we quantified the colocalization of OAT1/3 with DAPI across multiple confocal image stacks taken from cell-laden membranes.

We utilized representative cross-sectional fluorescent images and their corresponding intensity profiles from three different PToC models. The apical and basal sides of the cell monolayer were confirmed by brightfield imaging of the membrane and co-staining of the transporter protein with LTL, which is expressed on the apical side of the cell (Figure S6). The distance (Δd) between the positions of peak expression levels of each antibody and the DAPI peak, indicative of nuclei location, was measured. This approach allowed us to trace the polarity of transporter proteins within the epithelial layer (Figure 3B). Notably, #1-LTL+ PToC exhibited a clear basolateral polarization of OAT1 ($\Delta d < 0$). In contrast, OAT1 in #2-LTL+ PToC was distributed on both basolateral and apical sides, whereas RPTEC PToC predominantly expressed OAT1 slightly on the apical (Figure S7). This varied expression pattern likely explains the functional absence of OATs uptake or transport in RPTEC PToC[24] (Figure 3D). A similar trend was observed for OAT3, with clear basolateral polarization observed in #1-LTL+ PToC. #2-LTL+ PToC expressed OAT3 on both the apical and basolateral sides, while RPTEC PToC only exhibited slight expression of OAT3 on the apical side (Figure 3C).

To evaluate the functionality of OAT1 and OAT3, we employed fluorescein, an organic anion compound, and dye transported by both OAT1 and OAT3.[12] This evaluation was conducted using live confocal imaging and plate reader analysis (Figures 3D–3F).[25] The uptake and transport of fluorescein were examined both in the absence and presence of the OAT inhibitor probenecid (100 μM).[26] Notably, #1-LTL+ and #2-LTL+ PToC models demonstrated significantly higher fluorescein uptake compared to RPTEC in the absence of probenecid.

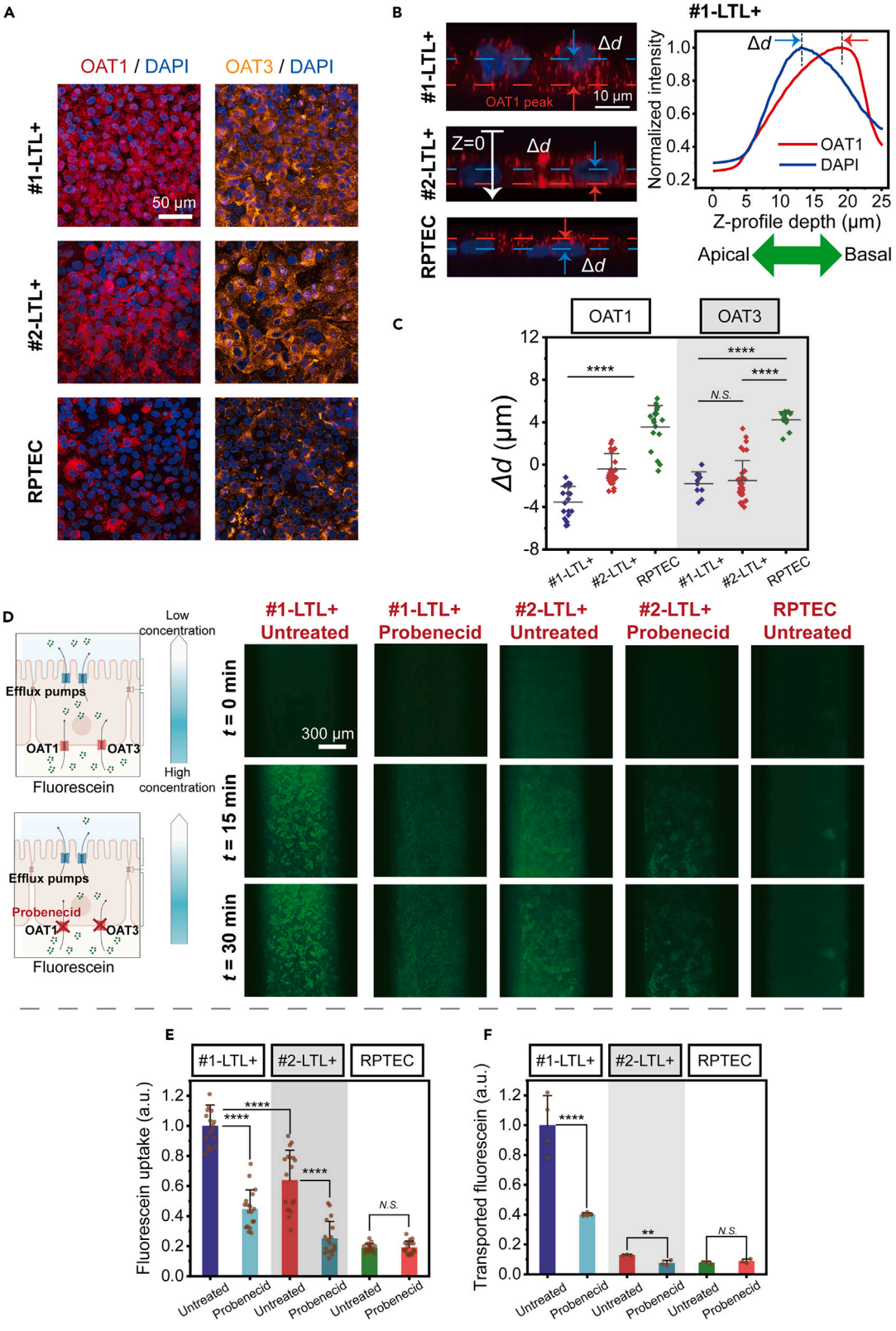
A
OAT1 / DAPI
OAT3 / DAPI
#1-LTL+
#2-LTL+
RPTEC
50 μm
B
#1-LTL+
#2-LTL+
RPTEC
Δd
OAT1 peak
10 μm
Z=0
#1-LTL+
Normalized intensity
1.0
0.8
0.6
0.4
0.2
0
5
10
15
20
25
Z-profile depth (μm)
OAT1
DAPI
Apical
Basal
C
OAT1
OAT3
Δd (μm)
12
8
4
0
-4
-8
****
****
****
N.S.
#1-LTL+
#2-LTL+
RPTEC
#1-LTL+
#2-LTL+
RPTEC
D
Low concentration
High concentration
Efflux pumps
OAT1
OAT3
Fluorescein
Efflux pumps
Probenecid
OAT1
OAT3
Fluorescein
#1-LTL+ Untreated
#1-LTL+ Probenecid
#2-LTL+ Untreated
#2-LTL+ Probenecid
RPTEC Untreated
t = 0 min
t = 15 min
t = 30 min
300 μm
E
#1-LTL+
#2-LTL+
RPTEC
Fluorescein uptake (a.u.)
1.2
1.0
0.8
0.6
0.4
0.2
0.0
****
****
****
****
N.S.
Untreated
Probenecid
Untreated
Probenecid
Untreated
Probenecid
F
#1-LTL+
#2-LTL+
RPTEC
Transported fluorescein (a.u.)
1.2
1.0
0.8
0.6
0.4
0.2
0.0
****
**
N.S.
Untreated
Probenecid
Untreated
Probenecid
Untreated
Probenecid

Figure 3. Enhanced expression and polarization of functional OAT1/3 in OPTCs

(A) Immunohistochemistry for OAT1 and OAT3 in #1-LTL+, #2-LTL+, and RPTEC tissue layers on day 5. Scale bars represent 50 μm.

(B) Select the cross-sectional fluorescent confocal image of the #1-LTL+, #2-LTL+, and RPTEC monolayer system, immunostained for OAT1, illustrating the definition of the relative distance of the protein of interest (e.g., OAT1 and OAT3) measured from the center of nuclei, scale bars represent 10 μm. Average PT-specific marker-to-nuclei distance in PToC seeded by #1-LTL+ cells for OAT1.

(C) Average PT-transporter-to-nuclei distance in #1-LTL+, #2-LTL+, and RPTEC monolayer system for OAT1 and OAT3. Kruskal-Wallis test with Dunn's post-test as follows: *, **, ***, ****, for $p \leq 0.05$, 0.01, 0.001, and 0.0001, respectively. Data are represented as mean ± SD ($n \geq 10$).

(D) Schematic of OAT1/3 substrate fluorescein uptake, transport, and inhibition by probenecid. Representative real-time images of the five different conditions. Scale bars represent 300 μm.

(E) Fluorescein uptake comparison among three cell sources tissue in the absence or presence of the probenecid at 30 min. Asterisks indicate *p*-values in the one-way ANOVA with Tukey's post-test as follows: *, **, ***, ****, for $p \leq 0.05$, 0.01, 0.001, and 0.0001, respectively. Data are represented as mean ± SD (n = 18, from 6 chips).

(F) Transported fluorescein comparison among three cell sources tissue in the absence or presence of the probenecid at 30 min. Welch's t-test, *, **, ***, ****, for $p \leq 0.05$, 0.01, 0.001, and 0.0001, respectively. Data are represented as mean ± SD ($n \geq 3$).

Upon introduction of probenecid, the normalized uptake values significantly decreased in #1-LTL+ and #2-LTL+, while RPTEC PToC showed negligible change under the same inhibition condition (Figures 3E and S8). #2-LTL+ PToC exhibited approximately 60% of the fluorescein uptake performance observed in #1-LTL+ PToC (Figure 3E). This reduction is attributed to the lower expression level or absence of polarization of OAT1/3 expression in #2-LTL+ PToC.

However, when we examine the transcellular transport of fluorescein by the plate reader, #2-LTL+ PToC plummeted to merely 10% of that observed in #1-LTL+ PToC (Figure 3F). This substantial difference compared to the uptake percentage is due to the higher passive diffusion permeability observed in #1-LTL+, as demonstrated in the inulin test (Figure 2D). Apart from this factor, the diminished function of efflux transporters is also a crucial contributing factor, which has piqued our interest in studying the OAT efflux system. Overall, these findings corroborate the establishment of functionally active hiPSC-derived kidney organoid source PToC models, especially highlighting their organic anion transport activity.

Comprehensive analysis of OAT1/3-mediated vectorial transport of substrates in OPTCs

To thoroughly investigate organic anion transport activity, we further assessed the comprehensive vectorial transport by analyzing the transcellular movement of OAT1 substrates adefovir and PAH, as well as the OAT3 substrate rosuvastatin across three chip types: #1-LTL+, #2-LTL+, and RPTEC, within the PToC model under different conditions (Figures 4A–4C).[27–29] We quantified the apparent permeabilities (P_{app}) for these substrates, noting both basal to apical transport (P_{app} (b → a)) and apical to basal transport (P_{app} (a → b)) across all substrates and PToC models, with #1-LTL+ showing notably higher basal to apical (b → a) transport (Figures 4D–4F and S9).

A key aspect of our study was the comparative analysis of basal to apical (b → a) transport in #1-LTL+ and #2-LTL+ within the PToC models. Notably, even though the basal to apical (b → a) transport in #2-LTL+ were much lower than those in #1-LTL+, and the efflux ratios (ER) for both models were remarkable (Figures 4G–4I). The ER, defined as the ratio of excretion to absorption rates, exceeded 2.0 for all three types of substrates (OAT1/3 mediated) in both #1-LTL+ and #2-LTL+ PToCs. This finding indicates a relatively smaller variance in ER between #1-LTL+ and #2-LTL+ PToCs, especially when considering PAH transport, where the difference in ER was not statistically significant (Figures 4G–4I). These observations underline the efficient active vectorial transport of OAT1/3 mediated substrates in OPTCs.

In the inhibition studies, upon adding probenecid (100 μM), both #1-LTL+ and #2-LTL+ demonstrated efficient inhibition of adefovir and PAH basal to apical (b → a) transport (Figures 4D, 4E, and 4J). Moreover, this inhibition had minimal impact on rosuvastatin transport in these models (Figures 4F and 4J). However, increasing the probenecid concentration to 500 μM[21] resulted in efficient inhibition of all three types of substrates in both OPTCs, especially near-complete inhibition of transport in #1-LTL+ (Figures 4D–4F, and 4J). By contrast, for RPTEC PToC, P_{app} shows a nonsignificant difference in either the b to a, a to b vectorial transport assay, or the inhibitor test (Figures 4D–4F and S10). Overall, both types of OPTCs demonstrate good inhibition performance, further highlighting the physiological relevance of the OPTC, especially for drug screening applications.

The effect of MK571 on efflux transport of OAT1/3 substrates

For a deeper comprehension of OAT1/3 uptake and efflux activities, #1-LTL+ stands out for its efficient transport of OAT1/3 substrates. This focus on #1-LTL+ PToC offers an opportunity to explore the contribution of the efflux system in mediating the transport of OAT1/3 substrates and to discern differences in the effects of probenecid and MK571 inhibition. The application of MK571, an established inhibitor of several multidrug resistance proteins in the efflux system, led to a notable increase in intracellular fluorescein accumulation, as demonstrated by heightened intracellular fluorescence intensity.[30] This accumulation, observed following the inhibition of fluorescein efflux, suggests the presence of MK571 inhibits the efflux transport process, specifically MRPs (Figures 5A and S7B). Intriguingly, the MK571 inhibitable efflux process also corresponded with a reduction in fluorescein's transcellular transport (Figure 5B).

To determine MK571 inhibitable efflux process specificity in mediating the efflux of OAT1 or OAT3 substrates, we executed a transcellular transport assay. This assay involved both OAT1 substrates (adefovir, PAH) and an OAT3 substrate (rosuvastatin), as depicted in Figures 5C and S11. Results from this assay indicated a significant impairment in the OAT1 excretion of adefovir and PAH upon MK571 inhibitable efflux

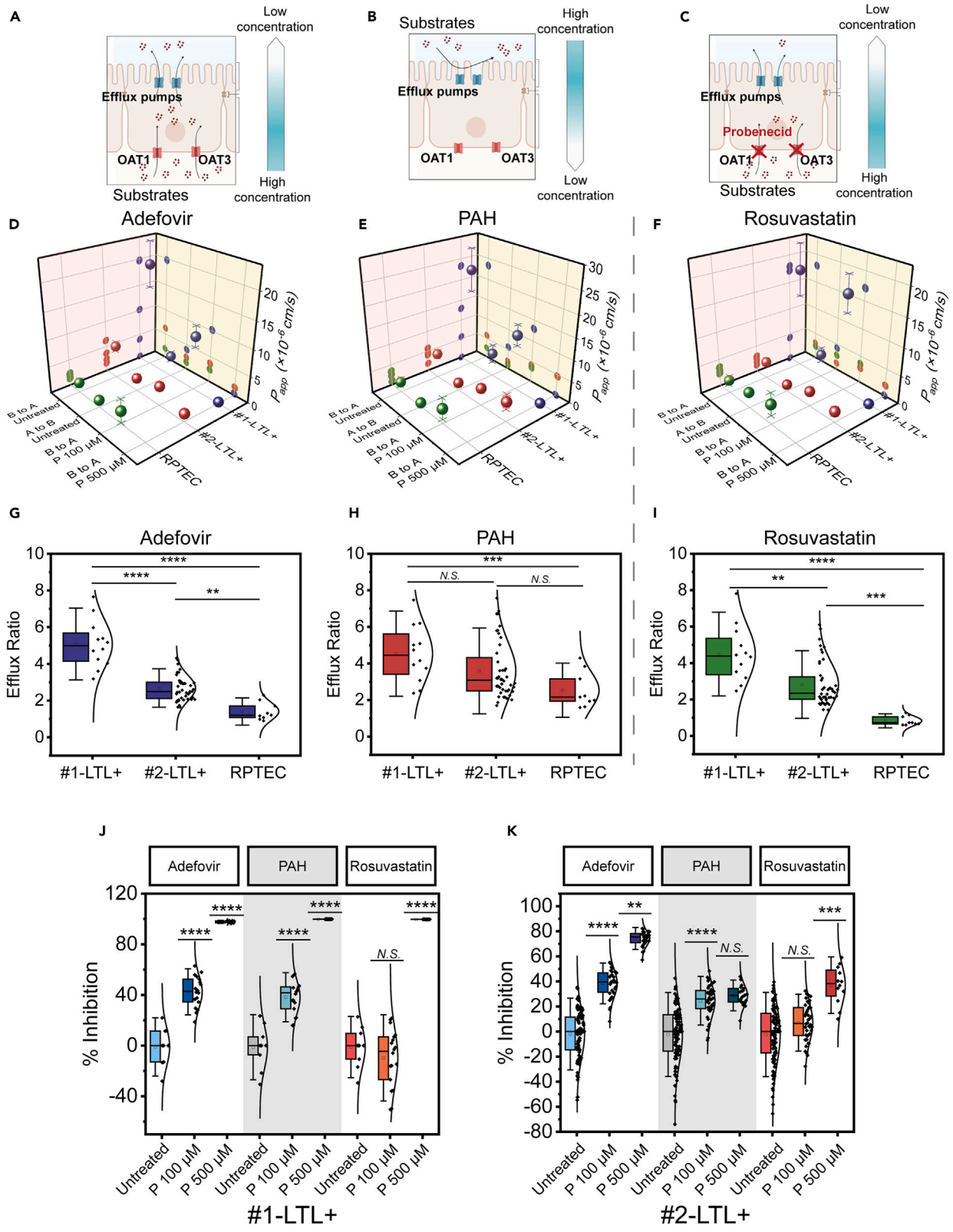
A
Low concentration
Efflux pumps
OAT1
OAT3
Substrates
High concentration
B
Substrates
High concentration
Efflux pumps
OAT1
OAT3
Low concentration
C
Low concentration
Efflux pumps
Probenecid
OAT1
OAT3
Substrates
High concentration
D
Adefovir
E
PAH
F
Rosuvastatin
B to A Untreated
A to B Untreated
B to A P 100 μM
B to A P 500 μM
RPTEC
#1-LTL+
#2-LTL+
Papp (×10-6 cm/s)
G
Adefovir
H
PAH
I
Rosuvastatin
Efflux Ratio
#1-LTL+
#2-LTL+
RPTEC
N.S.
J
Adefovir
PAH
Rosuvastatin
% Inhibition
Untreated
P 100 μM
P 500 μM
#1-LTL+
K
#2-LTL+

Figure 4. Comprehensive analysis of OAT1/3-mediated vectorial transport of substrates in OPTCs

(A–C) Schematic of OAT1/3—mediated fluorescein uptake, transport in both excretion (b-to-a) (A), and reverse (a-to-b) (B) directions and inhibition by probenecid (C).

(D–F) Apparent permeabilities (P_{app}) to (D) Adefovir, (E) PAH, (F) Rosuvastatin in both excretion (b-to-a) and reverse (a-to-b) directions by LC/MS. Probenecid, a chemical inhibitor for OAT transport, was applied to attenuate Adefovir uptake and efflux the function of OAT1/3. The pink projection represents the comparison of the same type of PToC under different conditions, while the yellow projection represents the comparison of different PToCs under the same conditions. Data are represented as mean ± SD ($n \geq 3$).

(G–I) Efflux ratio for (G) Adefovir, (H) PAH, (I) Rosuvastatin. Asterisks indicate *p*-values in the Kruskal-Wallis test with Dunn's post-test as follows: *, **, ***, ****, for $p \leq 0.05$, 0.01, 0.001, and 0.0001, respectively. Data are represented as mean ± SD ($n \geq 9$, from 3 to 11 chips).

(J) Inhibition of transcellular transport of Adefovir, PAH, and Rosuvastatin by probenecid (100 μM and 500 μM), in #1-LTL+ tissue and #2-LTL+ tissue. One-way ANOVA with Tukey's post-test as follows: *, **, ***, ****, for $p \leq 0.05$, 0.01, 0.001, and 0.0001, respectively. Data are represented as mean ± SD ($n \geq 9$, from 3 to 6 chips).

(K) Inhibition of transcellular transport of Adefovir, PAH, and Rosuvastatin by probenecid (100 μM and 500 μM), in #2-LTL+ tissue. Kruskal-Wallis test with Dunn's post-test as follows: *, **, ***, ****, for $p \leq 0.05$, 0.01, 0.001, and 0.0001, respectively. Data are represented as mean ± SD ($n \geq 40$, from 4 to 10 chips).

process. In contrast, the inhibition had no substantial effect on the OAT3 transport of rosuvastatin. These observations can be regarded as strong evidence for MK571 inhibitable efflux process specificity and underscore its pivotal role in the renal transport mechanisms associated with OATs.

Enhancement of OCT2 and P-gp functions in OPTCs allows improved drug screening and toxicity assessment

In addition to OAT1/3, OCT2 as the major influx transporters also play crucial roles. Similarly, MATE1 and P-gp serve as significant efflux transporters.[31,32] While MATE2-K also contributes to the efflux of OCT2 substrates (metformin), its expression compared to MATE1 is much lower.[33] Therefore, we investigated the capabilities of OPTCs in facilitating OCT2, MATE1, and P-gp functions, all of which are vital for drug screening. This phase aimed to assess how effectively the OPTCs can simulate these critical transport mechanisms and their implications in pharmacological applications. Immunohistochemistry revealed the expression of OCT2, MATE1, and P-gp (Figures 6A and S5B) in #1-LTL+, #2-LTL+, and RPTEC PToCs. Notably, all three PToCs exhibited these transporters, but their expression in RPTEC was significantly lower compared to #1-LTL+ and #2-LTL+ PToCs. Especially, the expression of MATE1 in RPTEC PToC was much lower than LTL+ PToCs, which caused the low OCT2 and MATE1 substrate metformin transcellular basal to apical (b → a) transport. Similar to the OAT function test, in the evaluations of metformin (Figures 6B and S12A) and quinidine (Figures 6C and S12B) transcellular basal to apical (b → a) transport, #1-LTL+ PToC showed the highest transport rates. #2-LTL+, while outperforming RPTEC in OCT2 and MATE1 functions, demonstrated a less basal to apical (b → a) transport rate in the quinidine test. However, upon conducting an ER analysis, both #1-LTL+ and #2-LTL+ PToCs demonstrated no significant differences in either metformin or quinidine transcellular transport assays (Figures S12C and S12D). This outcome is attributed to the lower non-specific passive diffusion observed in #2-LTL+ PToC, a finding corroborated by assays involving substrates of OATs.

In the final stage of our research, to comprehensively investigate the functionality of OATs and OCT2 in OPTC, we evaluated the impact of known nephrotoxins, such as cisplatin and aristolochic acid. Aristolochic acid is a potent nephrotoxin primarily transported basolaterally by OAT1 and OAT3.[34] Aristolochic acid (AA) was introduced into the basal reservoir and allowed to diffuse through the membrane for 24 h to assess its effects on #1-LTL+ and #2-LTL+ PToCs. Upon the introduction of 50 μM AA, both #1-LTL+ and #2-LTL+ PToCs exhibited significantly higher normalized lactate dehydrogenase (LDH) release compared to the control group without aristolochic acid (Figure 6D). Interestingly, #1-LTL+ demonstrated a markedly higher normalized LDH release compared to #2-LTL+. However, the untreated #1-LTL+ PToC displayed a higher baseline normalized LDH release compared to #2-LTL+ PToC, indicating an inherently higher rate of cell death in the #1-LTL+ PToC, consistent with our observations regarding its limited viability in long-term cultures (Figure 6D). These findings underscore the heightened physiological relevance of the OPTCs for drug screening and toxicity testing applications.

Cisplatin, known for its accumulation in the proximal tubule and resulting nephrotoxicity, is primarily taken up by the basolateral OCT2 transporter, leading to tubular injury through reactive oxygen species generation.[35] Upon introduction through the basal channel, cisplatin diffused readily, allowing proximal tubule cells to uptake the drug. Exposure to 100 μM cisplatin[36] elicited a higher normalized LDH response in both #1-LTL+ and #2-LTL+ compared to their respective untreated groups (Figure 6E).

The introduction of cimetidine (10 mM),[37] an OCT2 inhibitor,[38] for 24 h led to a significant reduction in LDH release in #1-LTL+, but its effect was less pronounced in #2-LTL+ under similar conditions. However, after refreshing the media and extending exposure to cimetidine for 48 h, a notable reduction in LDH release was observed in #2-LTL+ PToC. (Figure 6D). However, upon refreshing the media and extending the exposure to 48 h, the LDH release suddenly dropped, showing no difference among all conditions in #1-LTL+ PToC. This heightened sensitivity of #1-LTL+ PToC to cisplatin-induced nephrotoxicity is evident as most cells were already dead after 24 h (Figure S13A). This trend was consistently reflected in the LIVE/DEAD cell viability assays, where the majority of cells were found to be nonviable after 24 h of exposure to cisplatin in #1-LTL+ PToC. Additionally, the introduction of cimetidine resulted in a reduction in cell death (Figures S13A and S13C). These findings underscore the enhanced expression of OCT2 in OPTC, resulting in a physiologically relevant increase in drug uptake. This aspect highlights the potential of OPTC in drug screening and toxicity assessment, particularly for evaluating the impact of nephrotoxic compounds and the efficacy of OCT2 inhibitors.

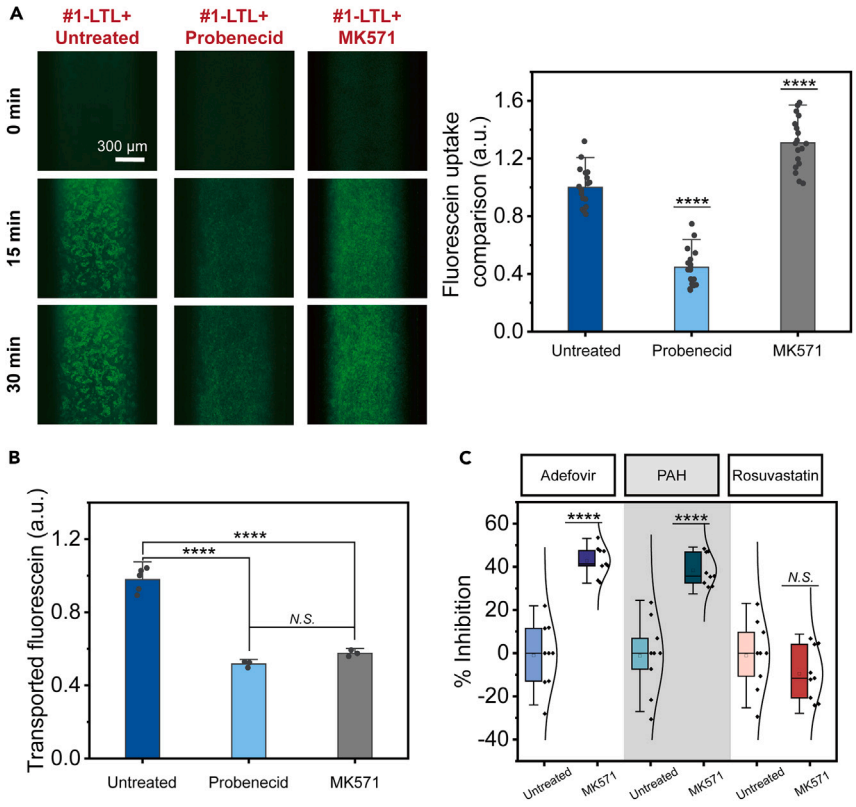

Figure 5. The effect of MK571 on efflux transport of OAT1/3 substrates

(A) Representative real-time images of the three different conditions. Scale bars represent 300 μm. And the Semi-quantification of fluorescein uptake comparison in the absence or presence of the inhibitors in #1-LTL+ tissue. From each single replicate, 6 different regions in focus were analyzed. Data are represented as mean ± SD (n = 18, from 6 chips).

(B) Transported fluorescein comparison among three conditions. Asterisks indicate *p*-values in the one-way ANOVA with Tukey's post-test as follows: *, **, ***, ****, for $p \leq 0.05$, 0.01, 0.001, and 0.0001, respectively. Data are represented as mean ± SD ($n \geq 3$).

(C) Inhibition performance studies of Adefovir, PAH, and Rosuvastatin transport by MK571 in #1-LTL+ tissue. Asterisks indicate *p*-values in the one-way ANOVA with Tukey's post-test as follows: *, **, ***, ****, for $p \leq 0.05$, 0.01, 0.001, and 0.0001, respectively. Data are represented as mean ± SD ($n \geq 9$, from 3 to 6 chips).

DISCUSSION

Together, our data demonstrate that the hiPSC-derived kidney organoid-based proximal tubule-on-chip is useful in the assessment of vectorial transcellular transport and nephrotoxicity, contributing significantly to renal physiology and pathophysiology research. The OPTC demonstrates enhanced expression and activity of key SLC proteins such as OAT1/3, OCT2, and the unidirectional efflux transporter MRPs, outperforming the RPTEC PToC. Their proficiency in simulating physiological drug transport and nephrotoxicity was especially apparent in handling compounds like adefovir, rosuvastatin, metformin, AA1, and cisplatin, highlighting their potential in drug screening and toxicity evaluation.

Previous studies have noted that cells cultured in 2D conditions often lose their characteristic morphology and exhibit leaky junctions.[39] When we cultured cells in our PToC device, we successfully maintained their cuboidal morphology and localizing tight junction proteins throughout the culture duration (Figure 2) compared to dish culture (Figures 2 and S4). Moreover, cells in the PToC device demonstrate notable epithelial polarization, as evidenced by OATs, OCT2, MATE1, and P-gp staining on their respective basolateral and apical surfaces. However, in comparing three different cell sources, we found distinct OAT expression patterns: #1-LTL+ exhibited a clear basolateral polarization, #2-LTL+ exhibited OAT1/3 expression on both apical and basal sides, and RPTEC showed only slightly apical expression. The observed functional impairment of OATs, attributed to incorrect polarization, and the downregulation of OAT expression, have resulted in diminished OAT function (Figures 3 and 4). These observations highlight the unique microenvironmental effects within our OPTC on cellular morphology, and the importance of correct cellular orientation and expression levels in maintaining functional transporter activity, which is crucial for accurate drug screening and nephrotoxicity studies.

To date, only a few *in vitro* models have recognized the value of organ-on-chip in enhancing *in vitro* proximal tubule models. Key examples include the use of P-gp in immortalized and primary RPTEC,[6,40] OAT1/3 in human primary RPTEC,[41] OAT1 and MRP4 in gene-modified ciPTEC,[12] OCT2/MATE1 in transfected MDCK cells.[42] However, none of the models have completely characterized the expression of these

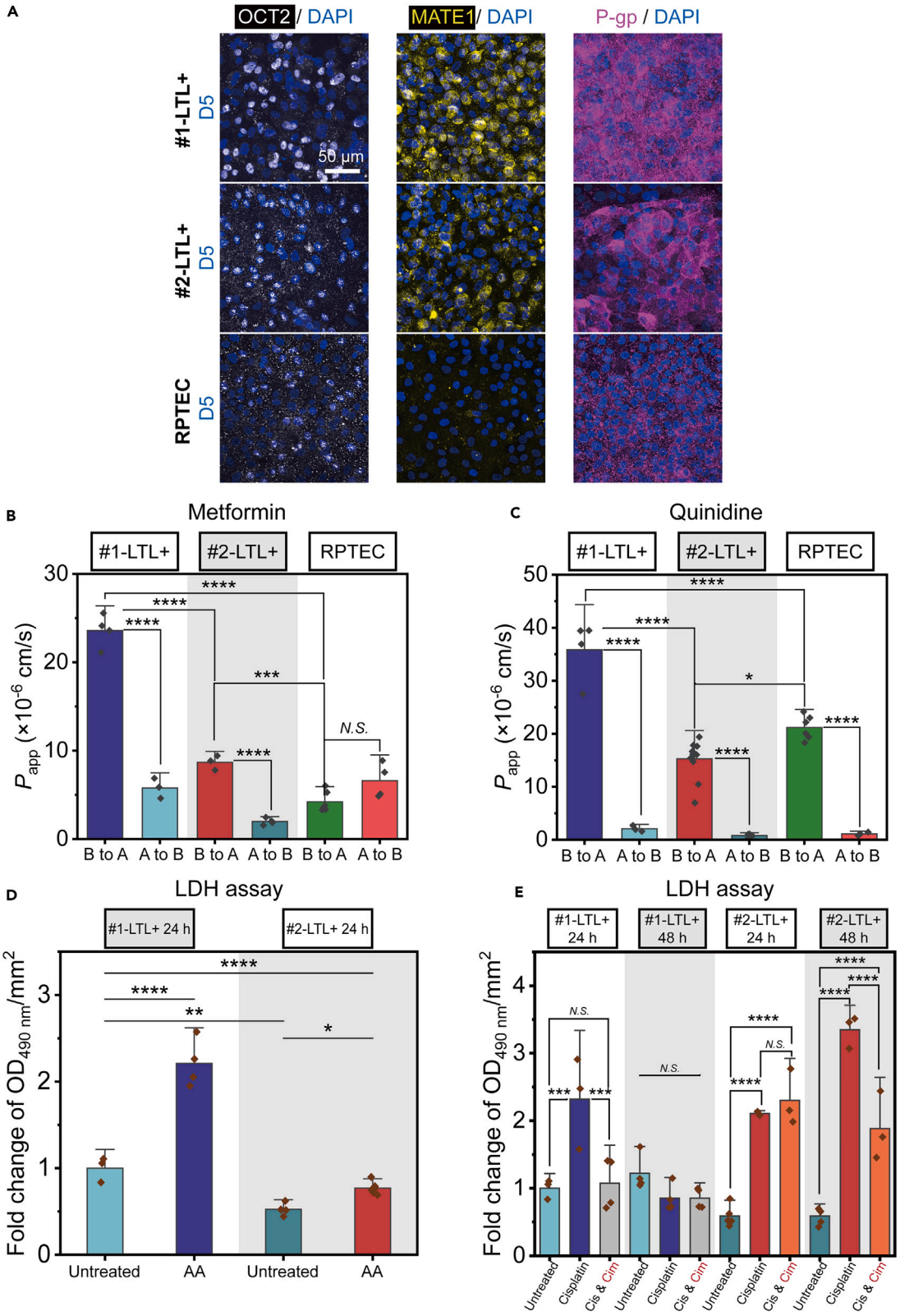
A
OCT2 / DAPI
MATE1 / DAPI
P-gp / DAPI
#1-LTL+ D5
#2-LTL+ D5
RPTEC D5
50 μm
B
Metformin
#1-LTL+
#2-LTL+
RPTEC
P_{app} (×10^{-6} cm/s)
B to A
A to B
N.S.
C
Quinidine
D
LDH assay
#1-LTL+ 24 h
#2-LTL+ 24 h
Fold change of OD$_{490\ nm}$/mm^2
Untreated
AA
E
LDH assay
#1-LTL+ 24 h
#1-LTL+ 48 h
#2-LTL+ 24 h
#2-LTL+ 48 h
Cisplatin
Cis & Cim

Figure 6. Enhancement of OCT2 and P-gp functions in OPTCs allows improved drug screening and toxicity assessment

(A) Immunohistochemistry for OCT2, MATE1, and P-gp in #1-LTL+, #2-LTL+, and RPTEC tissue layers on day 5. Scale bars represent 50 μm.

(B) Apparent permeabilities (P_{app}) to OCT2 and MATE1 substrate Metformin in #1-LTL+, #2-LTL+, and RPTEC PToCs. Data are represented as mean ± SD (n ≥ 3).

(C) Apparent permeabilities (P_{app}) to P-gp-mediated Quinidine by LC/MS in #1-LTL+, #2-LTL+, and RPTEC PToCs. Data are represented as mean ± SD (n ≥ 3).

(D) Normalized LDH release was observed after dosing the #1-LTL+ and #2-LTL+ PToCs with aristolochic acid for 24 h. Data are expressed as a fold change compared to the untreated condition and normalized by the #1-LTL+ untreated condition. Data are represented as mean ± SD (n ≥ 3).

(E) Normalized LDH release was observed after dosing the #1-LTL+ and #2-LTL+ PToCs with cisplatin for 24 h and 48 h in the presence or absence of cimetidine. Data are expressed as a fold change compared to the untreated condition and normalized by the #1-LTL+ 24 h untreated condition. Data are represented as mean ± SD (n ≥ 3).

Asterisks indicate *p*-values in the one-way ANOVA with Tukey's post-test as follows: *, **, ***, ****, for $p \leq 0.05$, 0.01, 0.001, and 0.0001, respectively.

important renal drug transporters and their potential to assess drug-drug interactions. These studies predominantly utilized animal or human primary proximal epithelial cells or immortalized cell lines rather than iPSC-derived sources. A major limitation of these approaches is the loss of vital transporter expressions post-cultivation in primary cells,[43] constraining their use for OAT1/3 or OCT2-mediated drug screening and pathology studies. Additionally, immortalized cell lines often lack the functional expression of these transporters. Models employing genetic modifications for functional expression are constrained to a single transporter,[44] limiting their utility in studying drug interactions. Furthermore, challenges arise in extrapolating data from non-human or immortalized cells to human *in vivo* conditions.

Our prior research[10] has highlighted the advantages of organ-on-chip and the use of iPSC-derived cells. However, the reliance on immortalized cells in these models has limited their ability to demonstrate OAT1/3 functions. To the best of our knowledge, apart from the work presented in this paper, no efforts have been made to create 2D functional tissues exclusively using hiPSC-derived epithelial cells. Although a 3D bioprinted proximal tubule model using iPSCs was reported for nephrotoxicity study,[21] the epithelial barrier was not tight enough to suppress passive diffusion of molecules. It limits quantitative analysis of vectorial transport across the PT layer or the efflux transport process.

Using the hiPSC-derived kidney organoid-based proximal tubule-on-chip 2D model, we were able to demonstrate that clinically relevant responses of the proximal tubule can be recapitulated. The first and most important is the maintenance of functions of OAT1/3 together with other key transporters with low barrier permeability. We showed that our OPTC not only assesses nephrotoxicity but also quantifies transcellular substrates transported specifically by OAT1, OAT3, OCT2, and P-gp. Furthermore, the organoid-based PT model effectively mimics transporter-mediated drug efflux with appropriate substrate specificity. This highlights the advantage of using iPSC-derived cells and a microfluidic system to replicate *in vivo* cellular transport mechanisms. Additionally, the simultaneous expression of multiple kidney transporters in our model will facilitate the examination of drug transporter systems and drug-drug interactions.

In selecting kidney organoid protocols, a detailed comparison between organoids that developed by Takasato et al. and Tsujimoto et al. reveal that, despite Tsujimoto et al.'s higher RNA-level expression of OAT1/3, its weaker basolateral polarization[24] leads to lower protein activity compared to Takasato et al. However, the higher passive diffusion permeability and baseline LDH release in #1-LTL+ suggest that #2-LTL+ has lower passive diffusion, forming tighter junctions, thus more suitable for long-term viability studies. This highlights the importance of protein activity over gene expression levels in iPSC cell application research. Future applications should consider these findings when selecting differentiation protocols. Currently, we utilized the initial iPSC cell line for each protocol, CRL 1502.3 for Takasato et al. and 4A6 for Tsujimoto et al., without considering the effects of different iPSC cell lines. Identifying the most suitable iPSC cell lines and optimizing differentiation protocols to enhance the expression of transporters will be crucial in the next steps for commercial applications.

In addition, incorporating iPSC-derived cells offers significant potential for modeling diseases using patient-derived iPSCs. This approach paves the way for creating precise, patient-specific proximal tubule models, enabling an in-depth study of the disease's unique pathophysiology. The use of patient-specific iPSCs marks a transformative step in kidney disease research, facilitating personalized disease modeling and potentially enhancing our understanding of disease progression and response to therapeutics. This innovative strategy will be a key focus in our forthcoming research on PT disease models.

Altogether, our study has successfully developed an OPTECs-on-Chip, which demonstrates an effective barrier function, enhanced expression of key renal transporters, and improved drug uptake and transport, especially for OAT1/3 and OCT2-mediated substances. This model, through a direct comparison of two popular kidney organoid differentiation protocols via vectorial transport function measurement and polarization analysis. Our findings highlight that the cell source based on Takasato et al. is superior for OAT1/3 and OCT2 studies, while the cell source based on Tsujimoto et al. is more suitable for nephrotoxicity studies requiring long-term incubation. In addition to gene expression levels, the polarity of the cells and correct localization of transporter proteins are critical considerations in transporter and nephrotoxicity studies. The OPTC offers surpasses traditional models in the potential of predicting drug clearance and nephrotoxicity, offering a more precise, and sensitive approach. Additionally, it advances basic research, and drug development leading to personalized tailored therapeutic strategies.

Limitations of the study

While our OPTC successfully recapitulates enhanced expression and activity of key SLC proteins such as OAT1/3, and OCT2, outperforming the RPTEC PToC, they remain immature compared with the *in vivo* condition. Our model's potential enhancements include upon perfusion with improvement in efflux pump expression polarization which is located apical side and incorporating iPSC-derived endothelial cells to create all iPSC-derived vascularized PT models, enhancing transporter expression and activity. Compared to other nephrotoxicity studies using organoids,[45] the concentration of cimetidine in the present study is much higher. This difference may result from drug absorption by

Polydimethylsiloxane (PDMS). Future steps will involve using lower concentrations of inhibitors or alternative materials with reduced drug absorption. Additionally, integrating advanced technical capabilities, such as real-time barrier function measurements using TEER electrodes, is crucial for making the model more applicable to preclinical drug development and drug-drug interaction studies. Although there is still room for improvement in our OPTC, our model is a valuable tool for DDI studies and drug development.

RESOURCE AVAILABILITY

Lead contact

Further information and requests for resources and reagents should be directed to and will be fulfilled by the lead contact, R.Y. (yokokawa.ryuji.8c@kyoto-u.ac.jp).

Materials availability

All unique/stable reagents generated in this study are available from the lead contact with a completed Materials Transfer Agreement.

Data and code availability

- The bulk RNA-seq data have been deposited at GEO and accession numbers are listed in the key resources table. RT-qPCR data reported in this paper will be shared by the lead contact upon reasonable request.
- This paper does not report the original code.
- Any additional information required to reanalyze the data reported in this paper is available from the lead contact upon request.

ACKNOWLEDGMENTS

This study was partially supported by the Japan Agency for Medical Research and Development (AMED-MPS) project under grants JP22be1004204 & JP17be0304205, and "Advanced Research Infrastructure for Materials and Nanotechnology in Japan (ARIM)" of the Ministry of Education, Culture, Sports, Science and Technology (MEXT) (Grant Number JPMX1222KT1172). All illustrations were created with BioRender.com. We thank S A Nyoman Putri Triantini, Megumi Kida, Aki Kubo, and Chizuru Inagaki for their assistance in lab support and facility usage.

AUTHOR CONTRIBUTIONS

C.M. and R.Y. designed research; R.Y. supervised the project; C.M., R.B.S., and R.Y. interpreted the data, and wrote the manuscript; C.M. and R.Y. conceived experiments and C.M. performed experiments; R.N. assisted with experiments. K.F. assisted in data interpretation and fabrication of the devices. T.A. and M.T. provided the protocols for culturing and maintenance of hiPSC-derived KOs, MACS, and assisted in data interpretation. N.I. provided scientific supervision on the substrates and inhibitors selection and assisted in data interpretation. All authors read, edited, and commented on the manuscript.

DECLARATION OF INTERESTS

R.Y., C.M., R.B.S., K.F., T.A., M.T., and R.N. are inventors on JP patent application no. 2024–73489 "Construction of proximal tubules micro-physiological system".

STAR★METHODS

Detailed methods are provided in the online version of this paper and include the following:

- KEY RESOURCES TABLE
- EXPERIMENTAL MODEL AND STUDY PARTICIPANT DETAILS
  - Kidney organoid development and culture
  - Proximal-tubule-on-chip system
  - RPTEC/TERT1 culture and seeding onto PToCs
- METHOD DETAILS
  - Device fabrication
  - Immunostaining and imaging
  - Quantitative RT-PCR
  - Diffusional permeability measurements
  - Fluorescein uptake and transport assay
  - Transcellular transport assay
  - Liquid chromatography–mass spectrometry (LC/MS)
  - Nephrotoxicity testing
  - LDH analysis
- QUANTIFICATION AND STATISTICAL ANALYSIS

SUPPLEMENTAL INFORMATION

Supplemental information can be found online at https://doi.org/10.1016/j.isci.2024.110760.

Received: May 2, 2024
Revised: June 24, 2024
Accepted: August 14, 2024
Published: August 19, 2024

REFERENCES

1. Keogh, J.P. (2012). Membrane Transporters in Drug Development. In Advances in Pharmacology (Academic Press Inc), pp. 1–42. https://doi.org/10.1016/B978-0-12-398339-8.00001-X.
2. US Food and Drug Administration (2012). Guidance for Industry Drug Interaction Studies-Study Design, Data Analysis, Implications for Dosing, and Labeling Recommendations DRAFT GUIDANCE.
3. Medicines Agency, E. (2012). Guideline on the Investigation of Drug Interactions.
4. Ministry of Health, L. and W (2014). Guideline on Drug Interaction for Drug Development and Appropriate Provision of Information.
5. Otani, N., Ouchi, M., Hayashi, K., Jutabha, P., and Anzai, N. (2017). Roles of organic anion transporters (OATs) in renal proximal tubules and their localization. Anat. Sci. Int. *92*, 200–206. https://doi.org/10.1007/s12565-016-0369-3.
6. Jang, K.J., Mehr, A.P., Hamilton, G.A., McPartlin, L.A., Chung, S., Suh, K.Y., and Ingber, D.E. (2013). Human kidney proximal tubule-on-a-chip for drug transport and nephrotoxicity assessment. Integr. Biol. *5*, 1119–1129. https://doi.org/10.1039/c3ib40049b.
7. Vedula, E.M., Alonso, J.L., Arnaout, M.A., and Charest, J.L. (2017). A microfluidic renal proximal tubule with active reabsorptive function. PLoS One *12*, e0184330. https://doi.org/10.1371/journal.pone.0184330.
8. Lin, N.Y.C., Homan, K.A., Robinson, S.S., Kolesky, D.B., Duarte, N., Moisan, A., and Lewis, J.A. (2019). Renal reabsorption in 3D vascularized proximal tubule models. Proc. Natl. Acad. Sci. USA *116*, 5399–5404. https://doi.org/10.1073/pnas.1815208116.
9. Sciancalepore, A.G., Sallustio, F., Girardo, S., Gioia Passione, L., Camposeo, A., Mele, E., Di Lorenzo, M., Costantino, V., Schena, F.P., and Pisignano, D. (2014). A bioartificial renal tubule device embedding human renal stem/progenitor cells. PLoS One *9*, e87496. https://doi.org/10.1371/journal.pone.0087496.
10. Banan Sadeghian, R., Ueno, R., Takata, Y., Kawakami, A., Ma, C., Araoka, T., Takasato, M., and Yokokawa, R. (2023). Cells sorted off hiPSC-derived kidney organoids coupled with immortalized cells reliably model the proximal tubule. Commun. Biol. *6*, 483. https://doi.org/10.1038/s42003-023-04862-7.
11. Nieskens, T.T.G., Peters, J.G.P., Schreurs, M.J., Smits, N., Woestenenk, R., Jansen, K., van der Made, T.K., Röring, M., Hilgendorf, C., Wilmer, M.J., and Masereeuw, R. (2016). A Human Renal Proximal Tubule Cell Line with Stable Organic Anion Transporter 1 and 3 Expression Predictive for Antiviral-Induced Toxicity. AAPS J. *18*, 465–475. https://doi.org/10.1208/s12248-016-9871-8.
12. Jansen, J., Fedecostante, M., Wilmer, M.J., Peters, J.G., Kreuser, U.M., Van Den Broek, P.H., Mensink, R.A., Boltje, T.J., Stamatialis, D., Wetzels, J.F., et al. (2016). Bioengineered kidney tubules efficiently excrete uremic toxins. Sci. Rep. *6*, 26715. https://doi.org/10.1038/srep26715.
13. Müller, F., Weitz, D., Mertsch, K., König, J., and Fromm, M.F. (2018). Importance of OCT2 and MATE1 for the Cimetidine–Metformin Interaction: Insights from Investigations of Polarized Transport in Single- And Double-Transfected MDCK Cells with a Focus on Perpetrator Disposition. Mol. Pharm. *15*, 3425–3433. https://doi.org/10.1021/acs.molpharmaceut.8b00416.
14. Takasato, M., Er, P.X., Chiu, H.S., and Little, M.H. (2016). Generation of kidney organoids from human pluripotent stem cells. Nat. Protoc. *11*, 1681–1692. https://doi.org/10.1038/nprot.2016.098.
15. Tsujimoto, H., Kasahara, T., Sueta, S.I., Araoka, T., Sakamoto, S., Okada, C., Mae, S.I., Nakajima, T., Okamoto, N., Taura, D., et al. (2020). A Modular Differentiation System Maps Multiple Human Kidney Lineages from Pluripotent Stem Cells. Cell Rep. *31*, 107476. https://doi.org/10.1016/j.celrep.2020.03.040.
16. Rizki-Safitri, A., Gupta, N., Hiratsuka, K., Kobayashi, K., Zhang, C., Ida, K., Satlin, L.M., and Morizane, R. (2022). Live functional assays reveal longitudinal maturation of transepithelial transport in kidney organoids. Front. Cell Dev. Biol. *10*, 978888. https://doi.org/10.3389/fcell.2022.978888.
17. van den Berg, C.W., Ritsma, L., Avramut, M.C., Wiersma, L.E., van den Berg, B.M., Leuning, D.G., Lievers, E., Koning, M., Vanslambrouck, J.M., Koster, A.J., et al. (2018). Renal Subcapsular Transplantation of PSC-Derived Kidney Organoids Induces Neo-vasculogenesis and Significant Glomerular and Tubular Maturation In Vivo. Stem Cell Rep. *10*, 751–765. https://doi.org/10.1016/j.stemcr.2018.01.041.
18. Romero-Guevara, R., Ioannides, A., and Xinaris, C. (2020). Kidney Organoids as Disease Models: Strengths, Weaknesses and Perspectives. Front. Physiol. *11*, 563981. https://doi.org/10.3389/fphys.2020.563981.
19. Ni, Z., Bikadi, Z., Rosenberg, M.F., and Mao, Q. (2010). Structure and Function of the Human Breast Cancer Resistance Protein (BCRP/ABCG2). Curr. Drug Metab. *11*, 603–617. https://doi.org/10.2174/138920010792927325.
20. Daoud, R., Kast, C., Gros, P., and Georges, E. (2000). Rhodamine 123 Binds to Multiple Sites in the Multidrug Resistance Protein (MRP1). Biochemistry *39*, 15344–15352. https://doi.org/10.1021/bi0020574.
21. Aceves, J.O., Heja, S., Kobayashi, K., Robinson, S.S., Miyoshi, T., Matsumoto, T., Schäffers, O.J.M., Morizane, R., and Lewis, J.A. (2022). 3D proximal tubule-on-chip model derived from kidney organoids with improved drug uptake. Sci. Rep. *12*, 14997. https://doi.org/10.1038/s41598-022-19293-3.
22. Uchimura, K., Wu, H., Yoshimura, Y., and Humphreys, B.D. (2020). Human Pluripotent Stem Cell-Derived Kidney Organoids with Improved Collecting Duct Maturation and Injury Modeling. Cell Rep. *33*, 108514. https://doi.org/10.1016/j.celrep.2020.108514.
23. Takasato, M., Er, P.X., Chiu, H.S., Maier, B., Baillie, G.J., Ferguson, C., Parton, R.G., Wolvetang, E.J., Roost, M.S., Chuva de Sousa Lopes, S.M., and Little, M.H. (2015). Kidney organoids from human iPS cells contain multiple lineages and model human nephrogenesis. Nature *526*, 564–568. https://doi.org/10.1038/nature15695.
24. You, G., and Morris, M.E. (2022). In DRUG TRANSPORTERS: Molecular Characterization and Role in Drug Disposition, Third Edition, G. You and M.E. Morris, eds. (Wiley), pp. 57–77. https://doi.org/10.1002/9781119739883.
25. Tabibzadeh, N., Satlin, L.M., Jain, S., and Morizane, R. (2023). Navigating the kidney organoid: insights into assessment and enhancement of nephron function. Am. J. Physiol. Renal Physiol. *325*, F695–F706. https://doi.org/10.1152/ajprenal.00166.2023.
26. Hagos, F.T., Daood, M.J., Ocque, J.A., Nolin, T.D., Bayir, H., Poloyac, S.M., Kochanek, P.M., Clark, R.S.B., and Empey, P.E. (2017). Probenecid, an organic anion transporter 1 and 3 inhibitor, increases plasma and brain exposure of *N* -acetylcysteine. Xenobiotica *47*, 346–353. https://doi.org/10.1080/00498254.2016.1187777.
27. Servais, A., Lechat, P., Zahr, N., Urien, S., Aymard, G., Jaudon, M.C., Deray, G., and Isnard Bagnis, C. (2005). Effet de l'inhibition des transporteurs OAT1 et MRP2 sur la clairance de l'adéfovir. Nephrol. Ther. *1*, 296–300. https://doi.org/10.1016/j.nephro.2005.06.011.
28. Nozaki, Y., Kusuhara, H., Kondo, T., Hasegawa, M., Shiroyanagi, Y., Nakazawa, H., Okano, T., and Sugiyama, Y. (2007). Characterization of the Uptake of Organic Anion Transporter (OAT) 1 and OAT3 Substrates by Human Kidney Slices. J. Pharmacol. Exp. Ther. *321*, 362–369. https://doi.org/10.1124/jpet.106.113076.
29. Windass, A.S., Lowes, S., Wang, Y., and Brown, C.D.A. (2007). The Contribution of Organic Anion Transporters OAT1 and OAT3 to the Renal Uptake of Rosuvastatin. J. Pharmacol. Exp. Ther. *322*, 1221–1227. https://doi.org/10.1124/jpet.107.125831.
30. Russel, F.G.M., Koenderink, J.B., and MASEREEUW, R. (2008). Multidrug resistance protein 4 (MRP4/ABCC4): a versatile efflux transporter for drugs and signalling molecules. Trends Pharmacol. Sci. *29*, 200–207. https://doi.org/10.1016/j.tips.2008.01.006.
31. Feng, B., LaPerle, J.L., Chang, G., and Varma, M.V.S. (2010). Renal clearance in drug discovery and development: molecular descriptors, drug transporters and disease state. Expert Opin. Drug Metab. Toxicol. *6*, 939–952. https://doi.org/10.1517/17425255.2010.482930.
32. Hillgren, K.M., Keppler, D., Zur, A.A., Giacomini, K.M., Stieger, B., Cass, C.E., and Zhang, L.; International Transporter Consortium (2013). Emerging Transporters of Clinical Importance: An Update From the International Transporter Consortium. Clin. Pharmacol. Ther. *94*, 52–63. https://doi.org/10.1038/clpt.2013.74.
33. Prasad, B., Johnson, K., Billington, S., Lee, C., Chung, G.W., Brown, C.D.A., Kelly, E.J., Himmelfarb, J., and Unadkat, J.D. (2016). Abundance of Drug Transporters in the Human Kidney Cortex as Quantified by Quantitative Targeted Proteomics. Drug Metab. Dispos. *44*, 1920–1924. https://doi.org/10.1124/dmd.116.072066.
34. Xue, X., Gong, L.-K., Maeda, K., Luan, Y., Qi, X.-M., Sugiyama, Y., and Ren, J. (2011). Critical Role of Organic Anion Transporters 1 and 3 in Kidney Accumulation and Toxicity of Aristolochic Acid I. Mol. Pharm. *8*, 2183–2192. https://doi.org/10.1021/mp100418u.
35. Arany, I., and Safirstein, R.L. (2003). Cisplatin nephrotoxicity. Semin. Nephrol. *23*, 460–464. https://doi.org/10.1016/S0270-9295(03)00089-5.
36. Soodvilai, S., Meetam, P., Siangjong, L., Chokchaisiri, R., Suksamrarn, A., and Soodvilai, S. (2020). Germacrone Reduces Cisplatin-Induced Toxicity of Renal Proximal Tubular Cells *via* Inhibition of Organic Cation

Transporter. Biol. Pharm. Bull. *43*, 1693–1698. https://doi.org/10.1248/bpb.b20-00392.

37. Ito, S., Kusuhara, H., Yokochi, M., Toyoshima, J., Inoue, K., Yuasa, H., and Sugiyama, Y. (2012). Competitive Inhibition of the Luminal Efflux by Multidrug and Toxin Extrusions, but Not Basolateral Uptake by Organic Cation Transporter 2, Is the Likely Mechanism Underlying the Pharmacokinetic Drug-Drug Interactions Caused by Cimetidine in the Kidney. J. Pharmacol. Exp. Ther. *340*, 393–403. https://doi.org/10.1124/jpet.111.184986.
38. Ludwig, T., Riethmüller, C., Gekle, M., Schwerdt, G., and Oberleithner, H. (2004). Nephrotoxicity of platinum complexes is related to basolateral organic cation transport. Kidney Int. *66*, 196–202. https://doi.org/10.1111/j.1523-1755.2004.00720.x.
39. Hoppensack, A., Kazanecki, C.C., Colter, D., Gosiewska, A., Schanz, J., Walles, H., and Schenke-Layland, K. (2014). A Human *In Vitro* Model That Mimics the Renal Proximal Tubule. Tissue Eng. Part C Methods *20*, 599–609. https://doi.org/10.1089/ten.tec.2013.0446.
40. Vriend, J., Peters, J.G.P., Nieskens, T.T.G., Škovroňová, R., Blaimschein, N., Schmidts, M., Roepman, R., Schirris, T.J.J., Russel, F.G.M., Masereeuw, R., and Wilmer, M.J. (2020). Flow stimulates drug transport in a human kidney proximal tubule-on-a-chip independent of primary cilia. Biochim. Biophys. Acta. Gen. Subj. *1864*, 129433. https://doi.org/10.1016/j.bbagen.2019.129433.
41. Weber, E.J., Chapron, A., Chapron, B.D., Voellinger, J.L., Lidberg, K.A., Yeung, C.K., Wang, Z., Yamaura, Y., Hailey, D.W., Neumann, T., et al. (2016). Development of a microphysiological model of human kidney proximal tubule function. Kidney Int. *90*, 627–637. https://doi.org/10.1016/j.kint.2016.06.011.
42. Jayagopal, A., Brakeman, P.R., Soler, P., Ferrell, N., Fissell, W., Kroetz, D.L., and Roy, S. (2019). Apical Shear Stress Enhanced Organic Cation Transport in Human OCT2/MATE1-Transfected Madin-Darby Canine Kidney Cells Involves Ciliary Sensing. J. Pharmacol. Exp. Ther. *369*, 523–530. https://doi.org/10.1124/jpet.118.255026.
43. Caetano-Pinto, P., and Stahl, S.H. (2023). Renal Organic Anion Transporters 1 and 3 In Vitro: Gone but Not Forgotten. Int. J. Mol. Sci. *24*, 15419. https://doi.org/10.3390/ijms242015419.
44. Zou, C., Romero, L., Turner, E., Shapiro, B.A., McWilliams-Koeppen, P., and Chase, B. (2024). Advanced renal cell models for drug toxicity screening.
45. Susa, K., Kobayashi, K., Galichon, P., Matsumoto, T., Tamura, A., Hiratsuka, K., Gupta, N.R., Yazdi, I.K., Bonventre, J.V., and Morizane, R. (2023). ATP/ADP biosensor organoids for drug nephrotoxicity assessment. Front. Cell Dev. Biol. *11*, 1138504. https://doi.org/10.3389/fcell.2023.1138504.
46. Toyohara, T., Mae, S.-I., Sueta, S.-I., Inoue, T., Yamagishi, Y., Kawamoto, T., Kasahara, T., Hoshina, A., Toyoda, T., Tanaka, H., et al. (2015). Cell Therapy Using Human Induced Pluripotent Stem Cell-Derived Renal Progenitors Ameliorates Acute Kidney Injury in Mice. Stem Cells Transl. Med. *4*, 980–992. https://doi.org/10.5966/sctm.2014-0219.
47. Schneider, C.A., Rasband, W.S., and Eliceiri, K.W. (2012). NIH Image to ImageJ: 25 years of image analysis. Nat. Methods *9*, 671–675. https://doi.org/10.1038/nmeth.2089.
48. Crowe, A., and Lemaire, M. (1998). In vitro and in situ absorption of SDZ-RAD using a human intestinal cell line (Caco-2) and a single pass perfusion model in rats: comparison with rapamycin. Pharm. Res. (N. Y.) *15*, 1666–1672. https://doi.org/10.1023/A:1011940108365.
49. Crivori, P., Reinach, B., Pezzetta, D., and Poggesi, I. (2006). Computational models for identifying potential P-glycoprotein substrates and inhibitors. Mol. Pharm. *3*, 33–44. https://doi.org/10.1021/mp050071a.

STAR★METHODS

KEY RESOURCES TABLE

REAGENT or RESOURCE	SOURCE	IDENTIFIER
Antibodies		
Anti-CD326 (EpCAM)	Miltenyi Biotec	130-113-263; RRID: AB_2726064
Anti-Lrp2/Megalin	Abcam	ab85626; RRID: AB_10674183
Anti-ZO-1	ThermoFisher	339100; RRID: AB_87181
LTL Biotinylated	Vector Labs	B-1325-2; RRID: AB_2336558
Anti-SLC22A6 (OAT1)	Abcam	ab135924; RRID: AB_3492058
Anti-SLC22A8 (OAT3)	Invitrogen Corporation	PA5105715; RRID: AB_2853899
Anti-Oct-2	Abcam	ab205482; RRID: AB_3492059
Anti-MATE-1	Abcam	ab170904; RRID: AB_2687930
Anti-P Glycoprotein	Abcam	ab92295; RRID: AB_2687930
Alexa Fluor 488 Donkey Anti-mouse IgG (H + L)	Thermo Fisher Scientific	CAT. # A21202; RRID: AB_141607
Alexa Fluor 647 Donkey Anti-mouse IgG (H + L)	Thermo Fisher Scientific	CAT. # A31571; RRID: AB_162542
Alexa Fluor 568 Donkey Anti-Rabbit IgG (H + L)	Thermo Fisher Scientific	CAT. # A10042; RRID: AB_2534017
Alexa Fluor 647 Donkey Anti-Rabbit IgG (H + L)	Thermo Fisher Scientific	CAT. # A31573; RRID: AB_2536183
Streptavidin, Alexa Fluor 647 conjugate	Thermo Fisher Scientific	CAT. # S32357; RRID: AB_2336066
Alexa Fluor 633 Donkey Anti-Goat IgG (H + L)	Thermo Fisher Scientific	CAT. # A21082; RRID: AB_2535739
Cellstain®- DAPI solution	dojindo	28718-90-3(DAPI)
Chemicals, peptides, and recombinant proteins		
Accumax	Innovative Cell Technologies	CAT. # AM105
A-83-01	Wako	CAT. # 035-24113
B-27 Supplement minus vitamin A	Thermo Fisher Scientific	CAT. # 12587001
BMP-4	PeproTech	CAT. # AF-120-05ET
BMP-7	R&D	CAT. # 354-BP
CHIR99021	Axon	CAT. # AXN-AXON1386-25
DMEM/F-12, GlutaMAX	Thermo Fisher Scientific	CAT. # 10565042
iMatrix-511 silk	Nippi	CAT. # 892021
KnockOut Serum Replacement	Thermo Fisher Scientific	CAT. # A3181502
CHIR99021	R&D	CAT. # 4423/10
APEL2	Stem Cell Technologies	CAT. # 05270
FGF9	R&D	CAT. # 273-F9-025
Heparin	Sigma-Aldrich	CAT. # 9045-22-1
Y27632	Wako	CAT. # 034-24024
Human FGF basic	WAKO	CAT. # 060-04543
NOGGIN	Peprotech	CAT. # 120-10C
Stem Fit AK02N	Takara Bio	CAT. # AK02N
Penicillin-Streptomycin	Thermo Fisher Scientific	CAT. # 15140122
Retinoic Acid	Sigma-Aldrich	CAT. #R2625
MEM Non-essential Amino Acids Solution (×100)	WAKO	CAT. # 139-15651
StemSureR 10 mmol/L 2-Mercaptoethanol Solution (×100)	WAKO	CAT. # 198-15781
Adeforvir	Sigma-Aldrich	SML0240

(*Continued on next page*)

Continued

REAGENT or RESOURCE	SOURCE	IDENTIFIER
p-Aminohippuric acid	Sigma-Aldrich	A1422
Rosuvastatin	Sigma-Aldrich	SML1264
Quinidine	Tokyo Chemical Industry Co., Ltd.	Q0006
Metformin	Tocris Bioscience	2864/100
Probenecid	Sigma-Aldrich	P876
MK571	Selleck	S8126
Fluorescein	Sigma-Aldrich	F245
Cimetidine	TCI America	C1252
Aristolochic acid I	Sigma-Aldrich	A5512
Cisplatin	TCI America	D3371
Critical commercial assays		
RNeasy Micro Kit	QIAGEN	CAT. # 74004
TaqMan™ Universal PCR Master Mix	Thermo Fisher Scientific	CAT. # 4364338
TaqMan primers: ACTB	Thermo Fisher Scientific	Hs01060665_g1
TaqMan primers: ABCC2	Thermo Fisher Scientific	Hs00960489_m1
TaqMan primers: ABCC4	Thermo Fisher Scientific	Hs00988721_m1
TaqMan primers: ABCB1	Thermo Fisher Scientific	Hs00184500_m1
TaqMan primers: SLC22A2	Thermo Fisher Scientific	Hs01010723_m1
TaqMan primers: LRP2	Thermo Fisher Scientific	Hs00189742_m1
TaqMan primers: SLC5A2	Thermo Fisher Scientific	Hs00894642_m1
Deposited data		
RNA sequencing data of kidney organoids	Takasato et al.[23]; Tsujimoto et al.[15]	GEO: GSE70101 GEO: GSE146119
Experimental models: cell lines		
4A6 (4A6C3-10)	Toyohara et al.[46]	N/A
CRL 1502.3	Takasato et al.[23]	N/A
RPTEC/TERT1	ATCC	CAT. # CRL-4031
Software and algorithms		
ImageJ 1.51u	Schneider et al.[47]	https://imagej.nih.gov/ij/
Microsoft Excel	https://products.office.com/home	Microsoft Office 365
OriginLab	https://www.originlab.com/	https://www.originlab.com/
FV31S-SW	https://www.olympus-lifescience.com/ja/downloads/detail-iframe/?0[downloads][id]=847252002	https://www.olympus-lifescience.com/ja/downloads/detail-iframe/?0[downloads][id]=847252002

EXPERIMENTAL MODEL AND STUDY PARTICIPANT DETAILS

Kidney organoid development and culture

Kidney organoids are prepared using the Takasato and Tsujimoto protocol, respectively.

For Takasato protocol, in brief, hiPSCs (female CRL1502.3 derived from ATCC CRL-1502 fetal fibroblast) are differentiated to the posterior primitive streak by activating canonical WNT signaling using glycogen synthase kinase (GSK-3) inhibitor, CHIR99021 (R&D, cat. no. 4423/10), in APEL2 medium (Stem Cell Technologies, cat. no. 05270). CHIR99021 was switched to 200 ng/mL FGF9 (R&D, cat. no. 273-F9-025) and 10 μg/mL heparin (Sigma-Aldrich) on day 5 to induce intermediate mesoderm. On day 7, 3D self-organization was initiated by culturing aggregates into a U-bottom low-attachment 96-well plate (MS-9096M, Sumitomo Bakelite) at a density of 300K cells/well and nephrogenesis was stimulated by 24 h pulse of 8 μM CHIR99021. The next day, the aggregates were transferred onto the Transwell cell culture plate (Corning, cat. no. 3450). FGF9 and heparin were withdrawn on day 12.[14,23]

For the Tsujimoto protocol, in brief, hiPSCs (4A6[46]) cultured under feeder-free conditions differentiated to create SIX2+ nephron progenitor cells until day 11. Induced NPCs were dissociated by incubation with Accumax (Innovative Cell Technologies, Inc.) and divided into an M-bottom low-attachment 96-well plate (MS-9096M, Sumitomo Bakelite) at a density of 200K cells/well. After 24 h of incubation (day 13),

the aggregates were transferred onto the Transwell cell culture plate (Corning, cat. no. 3450) followed by 10 days of air-liquid interface culture for the kidney organoid formation, as previously described.[15]

Proximal-tubule-on-chip system

In this research, pseudo proximal epithelia cells sorted from hiPSC-derived kidney organoids were seeded into the device to format the PToC. The organoids were harvested on day 26–28 and then sorted lotus tetragonolobus lectin positive cells (LTL+) using magnetic immunomagnetic cell separation (MACS).

For each experiment, around 40 organoids were prepared and dissociated using the enzymes provided in the Tumor Dissociation Kit (Miltenyi Biotec, #130-095-929). The dissociation buffer was made by dissolving the kit enzymes in a separation buffer. The separation buffer was prepared by mixing DPBS, (1X) (Gibco) EDTA (Fisher, 15575020) at 2 mM, and FBS at 0.5% (v/v). Dissociated cells were preserved on ice throughout the entire process before sorting. The cells were passed through a 10 μm pluriStrainer (pluriSelect, #43-50010-03) sieve to remove any remaining cell clusters. Then the cells were centrifuged and remixed with Biotinylated lotus tetragonolobus lectin (LTL), a robust proximal tubule brush border marker, which was applied to the suspension at a 1:100 ratio as the primary antibody. The sample was mixed well and refrigerated at 4°C for 30 min. After centrifuging and resuspending two times to completely remove any unattached antibody, mixed sample with Monoclonal Anti-Biotin MicroBeads (Miltenyi Biotec, #130-105-637), which were applied at a 1:5 ratio for indirect magnetic labeling. And then the suspension was incubated at 4°C for 30 min. The cells were gently applied to an MS Column (Miltenyi Biotec, #130-042-201) plugged into one of the eight slots of an OctoMACS separator (Miltenyi Biotec, #130-042-108). After the cell suspension was applied, rinsed the column with 500 μL of separation buffer to completely deplete the negative fraction (LTL–) (total volume 1.5 mL). Placed column on a collection tube, and immediately flushed with 1mL of separation buffer to collect the positive fraction (LTL+). The LTL+ cells were resuspended at 15×10^6 cell/mL in REGM (Renal Epithelial Growth medium, Lonza, CC-3190).

Then the LTL+ cells were seeded into the six-well plate (3335, Corning) with a coating of iMatrix-511 (0.5 mg mL^{-1}, Nippi, 892011/892012). After 4 to 5 days of culture, until they reached approximately ~90% confluency, the cells were trypsinized, resuspended at a concentration of 15×10^6 cells/mL in REGM (Lonza CC-3190), for the device seeding.

The chip microchannels and reservoirs were sterilized with 70% ethanol, dried under a clean bench, and exposed to UV light for 1 h. Prior to seeding, the membrane was coated by iMatrix-511 (0.5 mg mL–1, Nippi, 892011/892012) for 5 h. Before seeding, aspirate the coating from channels, and fill the bottom channel of each device with 200 μL of REGM. Then, 40 μL of the cell suspension was gently injected into the top channel. The devices were incubated at 37°C, in 5% CO_2 for 2 h until the cells were completely settled and attached to the membrane, after which 100 μL of REGM was added to the top channel reservoirs. The devices were maintained in the incubator, and both channels' media were refreshed daily.

RPTEC/TERT1 culture and seeding onto PToCs

Cryopreserved immortalized RPTEC/TERT1 cells (ATCC CRL-4031) were stored at a concentration of 10^6 cells/vial and cultured in T25 cell culture flasks in DMEM/F12 (Gibco 11320033) supplemented with the hTERT immortalized RPTEC growth kit (ATCC ACS4007) until they reached approximately ~90% confluency. After trypsinization, the cells were resuspended at a concentration of 15×10^6 cells/mL in REGM (Lonza CC-3190) and then seeded into chip microchannels. Before seeding, the membrane was coated with FNC Coating Mix (Athena 0407) and incubated at room temperature for 5 min. Other steps are the same as LTL+ cells device seeding.

METHOD DETAILS

Device fabrication

The proximal tubule-on-a-chip (PToC) device consisted of two identical slabs of Polydimethylsiloxane (PDMS, DuPont Toray Specialty Materials K.K.) with a porous PET membrane sandwiched between them. The PET membrane, featuring a pore size of 3.0 μm and a 5% porosity, was obtained from cell culture inserts (Corning). Microfluidic channels were patterned onto the top and bottom slabs using a standard SU-8 photolithography process on a Si (100) wafer, followed by casting and molding of the slabs. The dimensions of the channels were 1 mm in height, 1 mm in width, and 13.5 mm in length. After curing and demolding, a thin layer of uncured PDMS was spin-coated onto the bottom slab to act as an adhesion layer for the membrane. The top slab was then placed over the membrane to secure it in position. Subsequently, the slabs were bonded together such that the channels, separated by the membrane, aligned perfectly, and the device was left at 4°C for two days followed by overnight curing at 5°C to ensure optimal bonding. Upon bonding, 2 mm wide holes were punched through the slabs at both ends of the channels, and reservoirs were attached for culture medium storage.

Immunostaining and imaging

Cells on the top channel were fixed by applying 4% paraformaldehyde in DPBS for 15 min. The channel was then rinsed three times with DPBS to remove residual fixative and permeabilized with 0.1% Triton X-100 for 10 min. Subsequently, both channels were incubated in a blocking buffer containing 10% donkey serum for 1 h on a shaker at room temperature. Primary antibodies, prepared in fresh blocking buffer, were applied to the upper microchannel, and the samples were incubated overnight at 4°C. The following day, the channels were rinsed five times with DPBS for 5 min each, followed by incubation in a mixture of secondary antibodies in DPBS for 1 h at room temperature on the shaker. Finally, the upper channel membranes were treated with DAPI for 10 min, followed by antifade mountant (Fisher, S36937), and mounted on microscope slides. Confocal fluorescent microscopy was conducted using an Olympus FV3000 microscope. Image analysis was performed

using FV31S-SW (v2.5.1.228, Olympus) viewer software and ImageJ[47] (v1.53f51, NIH, USA). The concentrations of antibodies used are listed in Table S1.

Quantitative RT-PCR

Total mRNA was extracted and purified from three individual samples per condition using the NucleoSpin RNA isolation kit. Subsequently, 3 μg/100 μL of mRNA was utilized for reverse transcription with the PrimeScript RT Master Mix kit following the manufacturer's instructions. The resulting cDNA samples were then diluted (1:10) in TaqMan Universal PCR Master Mix along with TaqMan Gene Expression Assay forward and reverse primers specific to each gene of interest. These diluted samples were distributed into three wells of a 384 multi-well reaction plate. Quantitative RT-PCR was performed using the QuantStudio 5 Real-Time PCR detection system (ThermoFisher Scientific). β-actin was employed as the endogenous reference gene. Detailed primer information is provided in KRT.

Diffusional permeability measurements

The barrier function of the PToC models is assessed by measuring the diffusional permeability of FITC-labeled inulin (Sigma-Aldrich, F3272) because this compound is neither uptake nor secreted by PT *in vivo*. FITC-labeled inulin is dissolved in prewarmed REGM media at a concentration of 100 μg/mL and then applied in the top channel for all the conditions. The devices were soaked at 37°C and 100 μL samples were collected from the bottom channel at intervals and transferred into individual wells of a black bottom 96-well plate (Corning, CLS3925) at 1 h, 2 h, 3 h time points. Each well was pre-filled with REGM to achieve a working volume of 200 μL as suggested by the microplate reader's manufacturer. The bottom channel was topped up with 100 μL of REGM immediately after sampling. Prior to sampling, a single row of the 96-well plate was filled with FITC-labeled inulin solutions of known concentrations to obtain calibration data. The fluorescence emission of samples was measured by a microplate reader (Molecular Devices, SpectraMax iD5). We computed the time course concentration of inulin from the concentration of samples taken at each interval by reflecting the eliminated amount, using the following equation:

$$M_n = M_{n-1} + \frac{C_n \times 200\ \mu L - C_{n-1} \times 100\ \mu L}{1000} \quad \text{(Equation 1)}$$

$$P_d = \frac{M_n}{100\ \mu g/mL/2 \times 0.2\ mL} = \frac{M_n}{10\ \mu g} \quad \text{(Equation 2)}$$

where M_n and M_{n-1} represent transported inulin amount in the channel at current and previous sampling time points, respectively, units in μg. C_n and C_{n-1} are the corresponding sample concentrations all in μg ml^{-1}. The volumes 200 μL and 100 μL refer to the total channel and sampling volumes, respectively. P_d is the diffusional permeability ratio, assuming that the membrane is fully permeable, and diffusion is complete, half of the added inulin will diffuse to the bottom channel, i.e., 10 μg.

Fluorescein uptake and transport assay

To determine the OAT1/3 as well as MPR4 transport activity in hiPSC-derived kidney organoid-based and immortalized RPTEC/TERT1-based PToC, the fluorescein uptake and transport were assessed. To measure active fluorescein uptake in real-time, PToC was incubated at 37°C, in 5% CO_2 in a microscopy incubator (TOKAI HIT, STXG-IX3WX-SET) with 2 μM fluorescein (an OAT1/3 substrate, Sigma-Aldrich, F245) under the Confocal fluorescent microscopy (Olympus FV3000) in the presence or absence of specific drug transporter inhibitors. Background corrected data were normalized against fluorescein uptake at 0 min. Hoechst staining and z stack imaging were employed to create coronal views and determine the optimal z-height for assessing fluorescein uptake. Imaging began at approximately 50 μm from the apical side of the Hoechst-stained cells and extended to the membrane to ensure sufficient sample height for analysis. Pictures were taken every 2 min for a total duration of 30 min (Figure S14). The visual field was partitioned into six equally sized and positioned segments across all devices, with each segment analyzed as an individual region of interest. At least $N = 3$ independent devices (chips) per condition were used to collect measurement data.

To measure the transported fluorescein amount after 30 min, 100 μL samples were collected from the top channel at 30 min. And then measure the fluorescence density with a microplate reader same as diffusional permeability measurements.

Transcellular transport assay

The OAT1, OAT3, P-gp, and OCT2 activities in the hiPSC-derived kidney organoid-based and immortalized RPTEC/TERT1-based PToC were examined by quantifying the adefovir (an OAT1 substrate, Sigma-Aldrich, SML0240), PAH (*p*-Aminohippuric acid, an OAT1 substrate, Sigma-Aldrich, A1422), rosuvastatin (an OAT3 substrate, Sigma-Aldrich, SML1264), quinidine (an ABCB1 substrate, Tokyo Chemical Industry Co., Ltd., Q0006) and metformin (an OCT2 substrate, Tocris Bioscience, 2864/100). The hiPSC-derived kidney organoid-based or immortalized RPTEC/TERT1-based PToC washed with HBSS. The hiPSC-derived kidney organoid-based or immortalized RPTEC/TERT1-based PToC cells were preincubated at 37°C for 30 min with the top and bottom channels were filled with 200 μL of HBSS pH 6 and HBSS pH 7.4 respectively. OAT1/3 inhibitor (100 or 500 μM probenecid, Sigma-Aldrich, P876) or inhibitor of several multidrug resistance proteins (10 μM MK571, Selleck, S8126) were added to the bottom channel from the preincubation. After preincubation, 10 μM drug transporter substrates were added to the top or bottom channels. Sampling was conducted similarly to the diffusional permeability measurements procedure. Samples of 100 μL were

collected from the top or bottom channel at intervals and transferred into individual 1.5 mL Eppendorf tubes, replenished with 100 μL of HBSS pH 6 or HBSS pH 7.4 immediately after sampling. All samples were analyzed using an LCMS system (LCMS-8060NX Shimadzu).

We computed the time course concentration of substrates from the concentration of samples taken at each interval by reflecting the eliminated amount, using the following equation:

$$M_n = M_{n-1} + \frac{C_n \times 200\ \mu L - C_{n-1} \times 100\ \mu L}{1000} \quad \text{(Equation 3)}$$

where M_n and $M_{n\text{-}1}$ represent transported substrates amount in the channel at current and previous sampling time points, respectively, units in μg. C_n and C_{n-1} are the corresponding sample concentrations all in μg ml^{-1}. The volumes 200 μL and 100 μL refer to the total channel and sampling volumes, respectively.

$$P_{app}\ (cm/s) = \frac{\Delta Q/\Delta t}{60 \times A \times C_0} \quad \text{(Equation 4)}$$

where $\Delta Q/\Delta t$ is the filtration rate (nmol/min) which is the slope of regression straight line of transported substrates (nmol) versus time (min), C_0 is initial concentration in donor channel (μM) and A is the surface area of the channel (cm^2).[48]

$$\text{Efflux Ratio} = \frac{\text{basal to apical } P_{app}}{\text{apical to basal } P_{app}} \quad \text{(Equation 5)}$$

Efflux ratio was determined by dividing the basolateral to apical P_{app} by the apical to basolateral P_{app}. When the efflux ratio exceeds 2, the drug is considered as a substrate and the transporter surely transports the substrates.[49]

$$\%\ \text{Substrates inhibition} = \frac{P_{app}\ (\text{Untreated}) - P_{app}\ (\text{inhibition})}{P_{app}\ (\text{Untreated})} \times 100 \quad \text{(Equation 6)}$$

Where P_{app} (Untreated) is the P_{app} of substrates in the absence of test inhibitor, P_{app} (Untreated) is the P_{app} of substrates in the presence of test inhibitor.

Liquid chromatography–mass spectrometry (LC/MS)

The samples were collected from the supernatant, then immediately mixed with same volume of acetonitrile (FUJIFILM Wako). The mixed solutions were centrifuged for 5 min at 15,000 g. The samples were filtrated with a Cosmonice Filter (Nacalai Tesque), then analyzed by LC/MS to measure the concentration of adefovir, *para*-aminohippuric acid (PAH), rosuvastatin Ca, quinidine, and metformin according to a standard curve. LC/MS analysis was performed LCMS-8060NX (Shimadzu). The LC/MS methods are listed in Tables S2 and S3. The dwell time for each MRM transition was set at 100 ms.

Nephrotoxicity testing

All reservoirs and channels were supplied with fresh media prior to initiation. Subsequently, cisplatin (100 μM) or aristolochic acid (50 μM) was manually pipetted into the bottom channel, and the devices were then incubated at 37°C. After 24 h or 48 h, media from both the top and bottom channels were collected into a 1.5 mL Eppendorf tube. The collected luminal media samples were centrifuged at 5000 rcf for 5 min to eliminate cellular debris. Each supernatant was transferred to a fresh tube and stored at − 20°C for LDH assay analysis. For samples pretreated with the inhibitor, cimetidine (10 mM) was initially added to both the top and bottom channels, followed by incubation at 37 °C for 30 min. Subsequently, cisplatin was loaded in the presence of cimetidine in both channels, and sampling was conducted following the same procedure as the cisplatin group. The control group, referred to as the untreated group, was established without exposure to any drugs.

LDH analysis

LDH assays were conducted following the manufacturer's guidelines (Dojindo Laboratories, Cytotoxicity LDH Assay Kit-WST, 343–91753). Thawed media samples were prepared at 4°C, undergoing one freeze-thaw cycle. Subsequently, 50 μL of media from the top and bottom channels of each device were combined and transferred to a clear flat-bottom 96-well plate. Then, 100 μL of the Working Solution was added to each well, followed by incubation at room temperature for 30 min, while shielded from light. Upon completion, 50 μL of stop solution was introduced, any bubbles were eliminated using a syringe, and absorbance was measured at 490 nm using a plate reader. The normalized LDH release was adjusted based on the absorbance recorded from untreated #2-LTL+ cells at 24 h.

QUANTIFICATION AND STATISTICAL ANALYSIS

All bar graphs and dot plots are expressed as mean ± SD. Statistical analysis was done in OriginLab and differences between samples were considered statistically significant with a *p*-value below 0.05 when running a one-way ANOVA with Tukey's post-test for multiple comparisons and Welch's t-test for two groups for the sample data that follow a normal distribution. For the data that do not conform to a normal distribution, non-parametric method, the Kruskal-Wallis test with Dunn's post-test was employed.